https://doi.org/10.5194/essd-2025-718
Preprint. Discussion started: 15 January 2026

Open Access Earth System Science Data Discussions

GRACE and GRACE-FO Mascons for Ocean Dynamic Applications

Jennifer Bonin[1], Nadège Pie[2], Mark E. Tamisiea[2], Don Chambers[1], and Himanshu Save[2]

[1]College of Marine Science, University of South Florida, St. Petersburg, FL, 33701, USA
[2]Center for Space Research, University of Texas at Austin, Austin, TX, 78759-5321, USA

Correspondence to: Jennifer Bonin (jbonin@usf.edu)

Abstract. A new series of mascons are made from GRACE and GRACE-FO data, specifically designed for use by oceanographers interested in studying variations in ocean mass transport and circulation. This series has pre-removed those changes in ocean mass distribution caused by barystatic gravity, rotation, and deformation (GRD) signals, as well as the non-oceanographic signals caused by four major oceanic earthquakes, neither of which impact circulation. Subtle changes in the processing and regularization schemes also help reduce the visibility of instrument/orbital errors in the ocean signal, particularly in the arctic and near the sites of the removed earthquakes. The primary benefit of this data set is increased ease of use for researchers interested in ocean dynamics, as the product is designed to be used "off the shelf" with no additional corrections required, even by those less familiar with GRACE data usage. The complete dataset is available at https://doi.org/10.18738/T8/3VUPEW (Pie et al., 2025).

Short Summary. A GRACE/GRACE-FO mascon series is designed for studying ocean mass transport and circulation variations. Mass distribution changes caused by major oceanic earthquakes and barystatic gravity, rotation, and deformation (GRD) have been removed. Errors were reduced via processing and regularization changes, particularly in the arctic and near the removed earthquakes. This data set is designed for "off-the-shelf" oceanographic use.

1 Introduction

Since its launch in 2002, the Gravity Recovery and Climate Experiment (GRACE) and (since 2018) its Follow-On successor (GRACE-FO) have provided a unique view of the water mass exchange between the oceans, land, and cryosphere (Tapley et al., 2019). While hundreds of articles have used GRACE and GRACE-FO data (hereafter GRACE/FO) for studying important aspects of land hydrology (e.g.: Rodell & Reager, 2023) and the cryosphere (e.g.: Ciracì et al., 2020; Velicogna et al., 2020), the data can also be used for studying mass transport within the ocean (e.g., see Wahr et al., 1998 for the theoretical basis).

Some examples of ocean-focused studies include combining the mean geoid from GRACE with satellite altimetry to capture the surface geostrophic circulation (Tapley et al., 2003; Feng et al., 2013), quantifying seasonal and interannual mass exchanges in the North Pacific (Bingham & Hughes, 2006; Chambers & Willis, 2008; Song & Zlotnicki, 2008; Chambers,

https://doi.org/10.5194/essd-2025-718
Preprint. Discussion started: 15 January 2026

2011; Cheng et al., 2013), and investigating high frequency mass exchanges in the South Pacific (Boening et al., 2012). The data have also been used to study interannual large-scale mass exchanges between the Pacific and Indo-Atlantic ocean basins (Chambers & Willis, 2009), as well as transports of the Antarctic Circumpolar Current (Zlotnicki et al., 2007; Bergmann and Dobslaw, 2012; Makowski et al., 2015), Atlantic Meridional Overturning Circulation (Landerer et al., 2015), and Antarctic Bottom Water (Mazloff and Boening, 2016; Jeffree et al., 2024).

These studies all used either gridded spherical harmonic data or gridded ocean mascons (Save et al., 2012, 2016; Watkins et al., 2015; Wiese et al., 2016; Loomis et al., 2019) that contain both oceanographic and other geodetic signals unrelated to ocean dynamics, such as gravity, rotation, and deformation (GRD) signals (e.g., Farrell & Clark, 1976), global atmospheric pressure variations (e.g., Chambers & Schröter, 2011), as well as leakage from larger hydrology and ice sheet variations. Because GRD and leakage are largest near land and are significantly larger than ocean signals, the general recommendation has been to ignore GRACE/FO ocean grids within 300 km of land (e.g., Chambers, 2006; Chambers & Schröter, 2011) where these geodetic and leakage signals tend to be significantly larger than ocean signals. Even more problematic are large trends in the Indian Ocean and off the coast of Japan due to large earthquakes (Chao & Liau, 2019; Bonin et al, 2025). While most oceanographic studies utilizing GRACE/FO data have attempted to mitigate large geodetic signals by examining areas away from land and removing a global ocean monthly average (to remove the globally uniform, or barystatic, portion of the signal), others have not. These non-oceanographic signals likely contributed to some increased error in the results.

To improve the utility of GRACE/FO data for oceanographic applications, we have created a set of gridded mascons where non-oceanographic geodetic signals have been explicitly removed, leaving only signals from ocean mass variability that are most likely driven by ocean circulation changes. To accomplish this, we utilize the Center for Space Research release 6.2 (CSR RL06.2) mass concentration (mascon) processing stream (Save et al., 2016; Save, 2020) with alterations. The CSR RL06.2 processing stream already removes a model for glacial isostatic adjustment, restores a geocenter (degree 1) estimate, and replaces C_{20} and C_{30} with values based on satellite laser ranging (see details in Section 2).

For the dynamic ocean (DO) mascons that we have created (designated as the CSR RL06.2DO series), we modify the geocenter correction slightly and remove the barystatic-GRD signal for each month that results from the redistribution of mass between land and ocean (e.g., Tamisiea et al., 2010). We also remove solid earth mass change from four large oceanic earthquakes (Bonin et al., 2025) and we remove the global atmospheric pressure average over the ocean (Chambers & Schröter, 2011). The monthly barystatic-GRD signal is provided separately. Likewise, the earthquake model used is also provided so users can add it back and apply their own earthquake model. However, as discussed in Bonin et al. (2025), the earthquake signals as they appear in different mascon solutions vary considerably due to center-specific processing choices. Thus, the model we include is specific to the CSR processing and should not be used to remove earthquake signals from the JPL or GSFC mascons, or from any spherical harmonic solutions.

https://doi.org/10.5194/essd-2025-718
Preprint. Discussion started: 15 January 2026

Because of these changes, the CSR RL06.2DO mascons are not appropriate for comparisons with ocean bottom pressure gauges, as they omit the pressure impact of the atmosphere and barystatic-GRD signals, which are measurable by pressure recorders. Nor are they intended to be used for global sea level budget studies, as the sea-surface height changes associated with GRD are also present in satellite altimetry (Ponte et al, 2018) but have been removed from the DO mascons. We would recommend using the standard mascons for most sea level budget studies unless users are trying to separate GRD and dynamic ocean contributions. The DO mascons are designed primarily for ocean dynamic applications, such as computing bottom currents, mass redistribution due to circulation changes, or oceanic sources of polar motion. They also should be more useful for assimilation into oceanographic models, which typically do not model barystatic-GRD or global atmospheric pressure changes.

Section 2 will describe the specific methods and data used in the creation of the CSR RL06.2DO data, including descriptions of: the mascon processing scheme and how it differs from RL06.2 (Section 2.1); the changes to the regularization scheme and how those impact the land/ocean mask (Section 2.2); the removed earthquake model (Section 2.3); and the removed barystatic-GRD model (Section 2.4). Section 3 will describe the differences between the standard CSR RL06.2 and CSR RL06.2DO mascons, and the ECCOv4r4 state estimate, showing reduction in variance by removing the barystatic-GRD and earthquake signals and showing significant improvement in several coastal areas. Section 4 will conclude by discussing how these new DO mascons can be utilized in oceanographic applications without having to ignore (or approximate) non-oceanographic geodetic signals.

2 Data and Methods

The standard CSR GRACE/FO mascon series (Save et al., 2016; Save, 2020) are gridded products available over the entire globe, both land and ocean. Each of the equal-area 40,962 hexagonal (and 12 pentagonal) mascons are roughly 120 km in diameter and are subdivided into “land” and “ocean” sections when located along coastlines. Though the data is released on a uniform 1/4° grid, the true resolution of the data is ~200-300km, because the regularization uses information with ~200 km resolution and the mascon signal is still limited by the fundamental ~300 km spatial resolution defined by GRACE/FO’s orbit altitude. The regularization better reduces the anisotropic stripe-pattern errors typical of the GRACE/FO solutions. It also more precisely localizes large land/ice signals into land mascons, thus reducing the spread of those land-based signals into ocean areas which naturally contain much less mass variability (e.g., Watkins et al., 2015; Save et al., 2016).

The dynamic ocean mascons are created using a process (Section 2.1) that is very closely related to the CSR RL06.2/RL06.3 (Save et al., 2016; Save, 2020) mascon processing. (RL06.2 and RL06.3 do not differ in their general processing methods,

https://doi.org/10.5194/essd-2025-718
Preprint. Discussion started: 15 January 2026

though RL06.3 ingests different accelerometer data than RL06.2 and RL06.2DO in the later months). The estimation of the RL06.2 mascons is performed with respect to a background model that aims at representing most of the known time variable gravity signals: annual and semi-annual signals globally, plus trends in the icy regions of Greenland and Antarctica. This results in minimal peak shaving of these large signals during regularization, since the amplitude of the correction signal is roughly the same size over the entire land region (Save 2012). For the estimation of the RL06.2DO mascons, we modified the estimation background model so that it would also include mass signals from major earthquakes and a preliminary approximation of the barystatic-GRD effect associated with the linear trend of modern-day ice mass loss as measured by GRACE/FO. We also altered the sequence of when we apply the ellipsoidal correction relative to other corrections (e.g., the replacement of C_{20}/C_{30}). All these changes are described in Section 2.1.

Following the changes in the RL06.2DO estimation background, we modified the regularizing constraints applied in the CSR mascons' estimation, to reduce the estimation error in regions near large earthquake signals and to better localize the ocean signals and to reduce the impact of instrument and orbit errors in the Arctic Ocean. The Arctic constraint changes resulted in a slight change of the standard CSR land/ocean mask definition, such that the ocean-only DO mascon series excludes the Arctic islands of Franz Josef Land, which contain land areas experiencing measurable grounded-ice mass loss, but were treated as purely "ocean" mascons in the standard CSR mascon products. This is described in detail in Section 2.2.

Since the primary objective for the DO mascon is to remove non-oceanographic signals over the ocean, we also remove three new signals during or after the creation of the DO mascons. First, during the pre-processing, we model and remove the impact of four major earthquakes. Our earthquake model includes the very large 2004 Andaman-Sumatra earthquake (magnitude 9.2) in the Indian Ocean and the 2011 Tōhoku, Japan quake (magnitude 9.0), both of which are easily visible in the current GRACE/FO ocean mascons. This removes most of the solid earth signal in the ocean mascons that is not related to oceanographic processes. Section 2.3 describes this model.

Second, as a new post-processing step, we remove the precise monthly GRD pattern that results from mass exchange between the land and ocean, as computed from the estimated land DO mascons themselves (Section 2.4). While mass in the ocean is increasing as ice sheets melt (Chambers et al., 2017; Cazenave et al., 2019), the barystatic-GRD is a purely geodetic signal and has no direct relationship to physical processes in the ocean driven by wind and/or buoyancy fluxes. We also remove the monthly average over the global oceans of the restored GAD (Section 2.4), as this is caused by monthly-varying uniform atmospheric pressure changes over the ocean (Chambers & Schröter, 2011). Such a uniform pressure change will not cause any ocean dynamical signal.

Overall, the signal content of the DO mascons (over ocean grids only) can be approximately related to the original RL06.2 mascons by:

https://doi.org/10.5194/essd-2025-718
Preprint. Discussion started: 15 January 2026

$$RL06.2DO(x,y,t) \approx RL06.2(x,y,t) - GRD(x,y,t) - EQ(x,y,t) - GAD_{avg}(t) \quad (1)$$

where (x, y) are the spatial location, t is time, GRD refers to the barystatic-GRD mass estimate (released with the product), EQ refers to the earthquake mass estimate (released with the product), and GAD_{avg} is the monthly spatial average over the oceans of the standard GAD product (Dobslaw et al., 2017) released on the CSR mascon grid (available at https://download.csr.utexas.edu/outgoing/grace/RL0603_mascons/CSR_GRACE_GRACE-FO_RL0603_Mascons_GAD-component.nc; last access 3 Nov. 2025). The equation is not exact due to changes in regularization weights, masking, geocenter updates, and implementation of the ellipsoid correction, but it gets the idea across.

2.1 Alterations to Mascon Estimation Background Model and Processing

All the background models from the GRACE/FO CSR Level-2 RL06 Processing Standards documentation (Save, 2019) are already accounted for in the spherical harmonics normal equations of the official CSR RL06.2 Level-2 solutions, from which the mascon normal equations are derived. In particular, these background models include the GOT4.8 ocean tide model and the non-tidal atmospheric and ocean de-aliasing (AOD) model, AOD1B RL06 (Dobslaw et al., 2017). To further minimize estimation errors and peak-shaving due to regularization, CSR mascons are estimated with respect to an a priori background model which also includes most of the large known gravity signals. The background model used for the CSR RL06.2 mascons includes trends over large ice-covered regions, annual and semi-annual signals globally (both estimated from RL05 versions of GRACE/FO), and a glacial isostatic adjustment (GIA) based on the ICE-6G_D GIA model (Peltier et al., 2017). This estimation background model (excluding GIA contribution) is restored prior to release.

The background model used for the estimation of the RL06.2DO mascons builds on the one used for RL06.2 mascons by adding an earthquake model and a preliminary barystatic-GRD model that complements the expected ice mass trend. The earthquake model, described in Section 2.3, was derived from the standard RL06.2 CSR mascons, in an iterative process. It accounts for the signals from the large earthquakes in Andaman Bay and near Japan over the GRACE/FO period. Because RL06.2 and RL06.3 do not model the large amplitude of these earthquake signals, the constraints applied near the earthquake regions have to be very “loose” for the regularization to adjust for that amplitude. If the constraints are not left loose enough, the earthquake signal will leak into other neighbouring mascons, corrupting the ocean and hydrology signals. Moreover, incorporating the huge (50-100 cm) jump caused by the co-seismic solid earth signal of the earthquakes into the mascons requires the use of extremely loose regional constraints, which increase the noise in near-earthquake mascons by an order of magnitude over other ocean mascons (Bonin et al., 2025). By removing most of the earthquake signal as a pre-processing background model, we have largely remedied this in the DO mascons, resulting in a better solution both locally and globally.

https://doi.org/10.5194/essd-2025-718
Preprint. Discussion started: 15 January 2026


Open Access Earth System Science Data Discussions

Second, the large mass loss from ice-covered regions corresponds to a barystatic-GRD ocean mass trend which is very apparent in RL06.2 ocean mascons, particularly near the coasts of Greenland and Antarctica. In the DO mascons, a preliminary barystatic-GRD model is added to the background, computed as the response to a long-term linear ice mass trend estimate already included in the RL06.2 background model. This calculation is less complete than our final barystatic-GRD estimate, described in Section 2.4, which we remove from the DO mascons during post-processing. The preliminary estimate is only driven by an estimate of ice mass trend. Removing the majority of this known signal helps during mascon estimation because the tighter ocean constraints may not allow for the GRD signal to adjust into the ocean regions correctly. We found that its primary impact was to enable larger ocean mass trend estimates in the immediate vicinity of the ice sheets, where the GRD signal is the largest. This preliminary GRD model is restored at the end of the estimation process.

In addition to these major changes in the background model, we have also made more subtle changes to the CSR mascon processing scheme. In the standard RL06.2 (and RL06.3) CSR mascon processing, an ellipsoid correction accounting for the true shape of the Earth (Ditmar, 2018) is applied to the mascon estimates before other corrections are applied. The ellipsoid-corrected RL06.2 mascons estimates are then altered so that the contributions of the C_{20} and C_{30} terms (converted to water layer grids) are replaced with values based on satellite laser ranging (SLR) using GRACE TN-14 (Loomis et al., 2020), and a geocenter degree 1 estimate is added using GRACE TN-13 (Sun et al., 2016). Finally, a GIA model (ICE6G-D; Peltier et al., 2017) is removed from the mascon grids and the standard CSR Level-2 GAD (which represents the AOD1B model over the oceans (Dobslaw et al., 2017)) is added back, leading to the fully-corrected RL06.2 mascons.

When creating the DO mascon series, we revised the order of corrections applied to the standard CSR mascons. The replacement of C_{20}/C_{30}, the addition of the geocenter terms, and the removal of GIA geopotential are now done prior to the ellipsoidal correction, because these terms are expressed on a spherical Earth and should not be applied directly to a field expressed on an ellipsoid Earth. Also, as specified in Ditmar (2018), the ellipsoid correction applies to the 2-D surface mass anomalies only and not to the solid Earth mass transport, which occurs much deeper (tens to hundreds of km deep). Therefore, it is necessary to remove such signals from the mascons prior to applying the ellipsoid correction. Aside from their order with respect to the ellipsoidal correction, corrections of the C_{20} and C_{30} terms and GIA were kept the same as those applied to the RL06.2 mascons.

Just as there is a different version of TN-13 for each SDS spherical harmonic distribution, the mascons should have a degree 1 contribution that is consistent with the rest of its mass change distribution, a strategy currently used in the JPL mascons. As we want to estimate and remove a barystatic-GRD estimate, it is easy to simultaneously estimate the degree 1 contribution, similar to Sun et al. (2016) and Swenson et al. (2008). An intermediary set of mascons (after the ellipsoidal correction), used

https://doi.org/10.5194/essd-2025-718
Preprint. Discussion started: 15 January 2026


Open Access Earth System Science Data Discussions

in the barystatic-GRD calculation, includes the TN-13 correction designed for CSR's L2 spherical harmonic solution. After the new degree 1 contribution is estimated, it replaces the TN-13 values, and the ellipsoidal correction is recalculated.

2.2 Alteration of Regularization Constraints:

All CSR mascons are regularized (Save et al., 2012, 2016), with constraints that vary in different areas of the world, and even at different times of the year. Regularizing constraints are represented as sigmas (standard deviations) because they are connected to the expected variance of the signal in the region, such that lower values of sigma mean constraints that tightly limit the estimate, and higher sigma values mean looser constraints that allow the estimate more flexibility to adjust and hold larger signal variability. Sigma values over land are higher than those in the ocean (typical land sigmas are ~10-30 cm, while ocean sigmas are ~3-5 cm), as land/ice variability is expected to be higher than ocean signal variability.

The first major regularization constraint change in the DO mascons was to tighten the very loose constraints in Andaman Bay and near Japan back to "normal" ocean constraint levels. While RL06.2 used very large regularizing sigmas in those localized regions to let in the earthquake signals and not smear them over large spatial scales, estimating the DO mascons with respect to a background model that already includes these large signals eliminates the need for such an accommodation in the constraints. Therefore, the RL06.2DO ocean mascon constraints near the earthquake epicenters are defined as they are in the rest of the global ocean, with typical values between 3-5 cm (since the regularization does not have to adjust the large earthquake signals anymore).

The second major change in the definition of the regularization constraint was implemented over the Arctic Ocean region. In the previous CSR mascons, up through the RL06.1 release, the arctic ocean mascon constraints were in part defined by a 12-month climatology based on the older RL05 CSR mascons (Fig. A1). During early research in creating the DO mascons, we determined that the residual north/south stripe errors present in this climatology resulted in physically unrealistic striations in the Arctic Ocean (Fig. 1a), which were very unlikely to represent real ocean signal. These errors are largest near the poles and were particularly noticeable over the Arctic Ocean. As a result of our investigations, in CSR mascon series RL06.2 and RL06.3, the constraint definition was changed over the Arctic Ocean to exclude this GRACE-based climatology, using only a 12-month climatology defined by the GAD values from the AOD1B product, which cannot contain GRACE-style stripe errors. A lower-bound for the constraint sigmas was set to 3 cm (to prevent the GAD series from understating real signal) and an upper-bound set to 5 cm. This removed the unrealistic Arctic striations, while still allowing the constraints to vary realistically and seasonally (Figs. 1b and A2).

https://doi.org/10.5194/essd-2025-718
Preprint. Discussion started: 15 January 2026

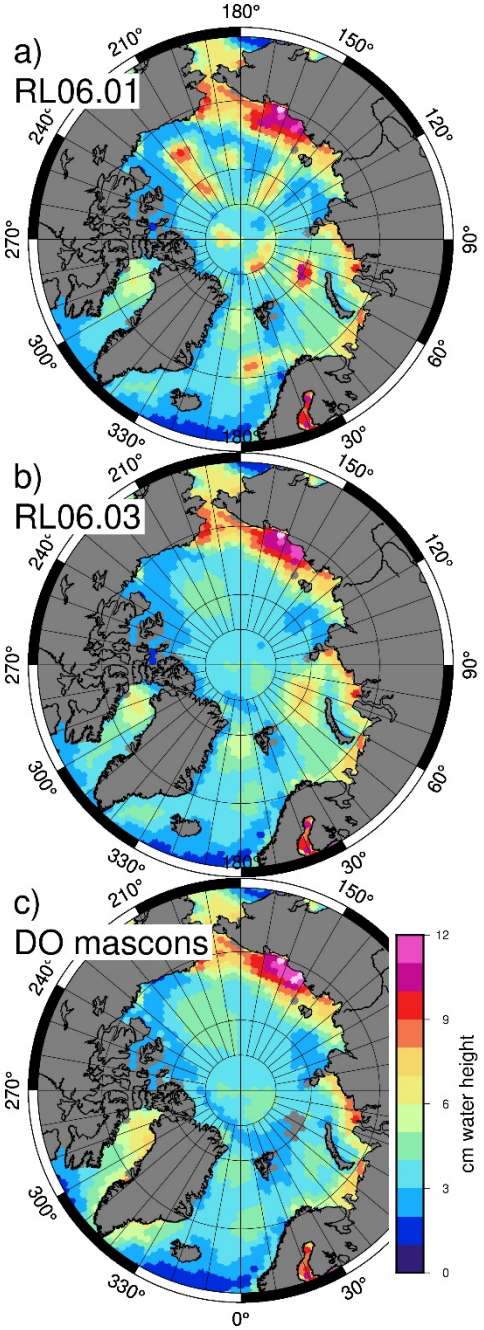

Figure 1: Signal RMS over the ocean of (a) CSR RL06.1 mascons, (b) CSR RL06.3 mascons, and (c) the dynamic ocean mascons with barystatic-GRD, EQ, and GAD_{avg} restored.

There is substantial variation in the actual Arctic Ocean signal which is not captured by a simple climatology (e.g., Fig. 2). In months when the real signal is substantially smaller than the climatological expectation, the RL06.3-style regularization

https://doi.org/10.5194/essd-2025-718
Preprint. Discussion started: 15 January 2026

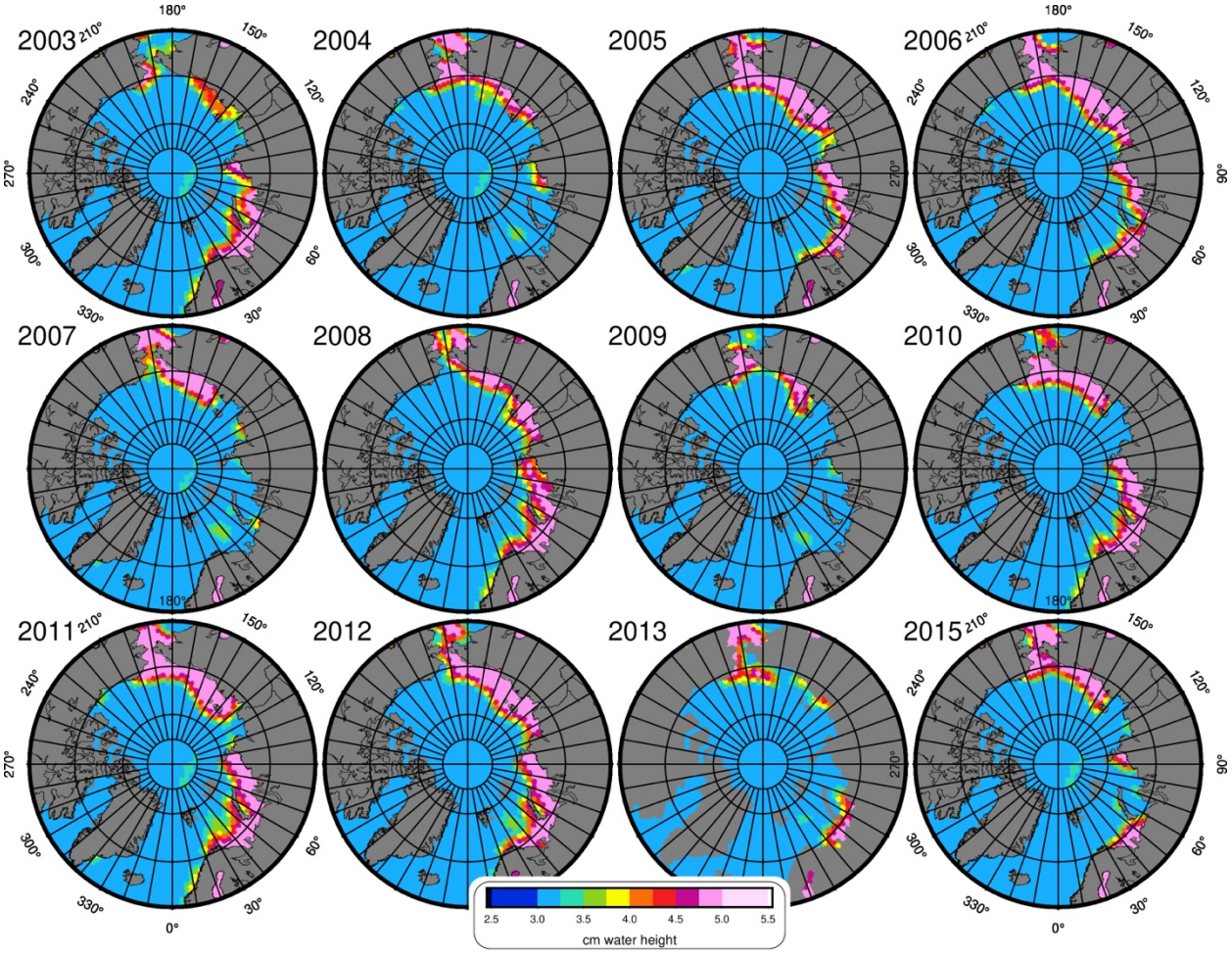

Figure 2: Examples of variability in constraint sigmas for RL06.2DO: first twelve February months. Unlike the RL06.2 constraints, the DO sigmas are not identical per month over the years.

https://doi.org/10.5194/essd-2025-718
Preprint. Discussion started: 15 January 2026

Open Access Earth System Science Data Discussions

The ocean variability which results from these constraint changes (Fig. 1c) is still quite close to that of the RL06.3 mascons (Fig. 1b). However, during our exploratory work into defining these new constraints, we noted that after removing the GRACE-based climatology from the Arctic Ocean constraints, a region of extremely high variability remained around 60°E (Fig. 1b). The majority of this signal is caused by a near-linear trend (Fig. 3a), which is considerably larger than trends elsewhere in the Arctic Ocean and does not have a known oceanographic explanation. This mass-losing region of the Arctic Ocean lies on top of Franz Josef Land (Fig. 3c), an icy archipelago that is 85% glaciated and strongly suspected to be a place of land ice mass loss (Jacob et al., 2012; Zheng et al., 2018; Schmidt et al., 2025). In all former GRACE/FO mascons (including CSR RL06.3 and the JPL and GSFC mascons), mascons overlaying Franz Josef Land have been officially considered "ocean", rather than "land", since they are more ocean than land, area-wise. In the CSR methodology, this means that the eight mascons covering these islands (yellow grids in Fig. 3d) had been assigned the very tight constraints applied to ocean mascons. However, if these areas are truly losing land-ice mass at a large rate, then by tightly constraining the signal, that mass loss will not be able to be contained in the local area but will instead leak out into the broader ocean area, which is what we observe in RL06.3 (Fig. 3a).

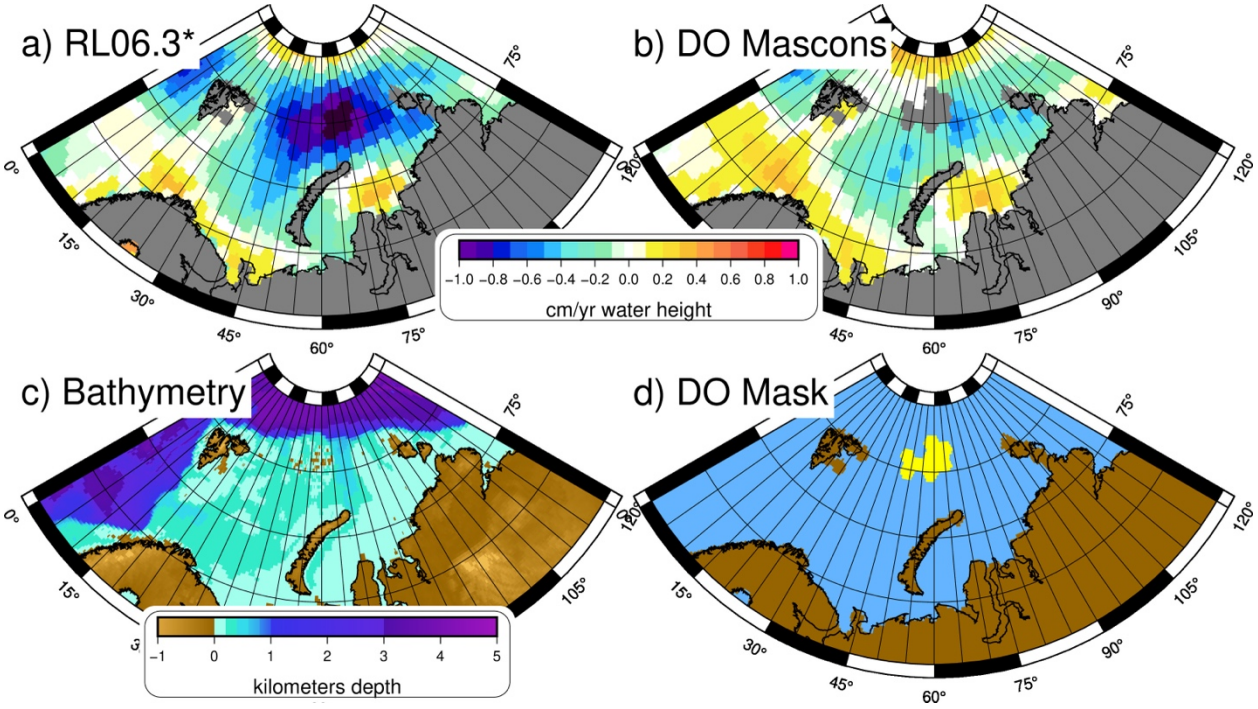

Figure 3: Trends of (a) the CSR RL06.3 mascons, after an appropriate GRD series and GAD_{avg} have been removed, and (b) the DO mascons. The ETOPO1 bathymetry (c) shows the location of Franz Josef Land, which is masked as "land" (yellow) in the DO mascons (d).

https://doi.org/10.5194/essd-2025-718
Preprint. Discussion started: 15 January 2026

In the DO mascons, we instead denote these eight mascons as "land", assigning them looser constraints based on the normal CSR land constraint definition. The "land" constraint sigmas over these island mascons typically vary between 4-8 cm over the lifetime of the mission. Redefining these eight mascons as "land" greatly reduced the trend (Fig. 3b) and RMS variability (Fig. 1c) in nearby ocean mascons, compared to the RL06.3 series. When we consider the average over a box around the Franz Joseph Land islands (Fig. 4), we find a much smaller trend for the DO mascons than for the CSR RL06.3 mascons (-1.88 mm yr^{-1} vs -6.48 mm^{-1} from 2002-2024). The remaining mass loss in the DO mascons lies on the new Franz Josef Land non-ocean mascons. We believe that this demonstrates a processing improvement, a more correct partitioning of land-ice signal away from ocean areas and presume that the nearby ocean mascons contain a lower amount of leakage error due to this constraint change. With that said, users are still advised that ocean mascons near the Franz Joseph Land mascons likely still contain some leaked signal and just be used with caution for oceanographic studies

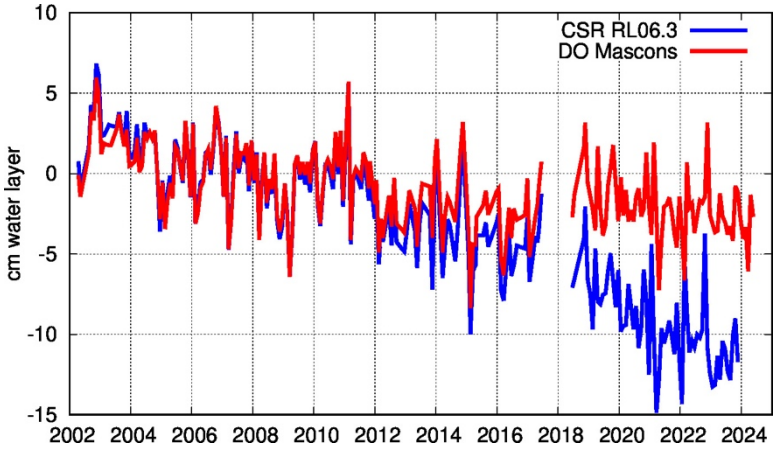

Figure 4: Average mass loss near Franz Josef Land over DO-defined ocean mascons only (latitudes 35°-80°E and longitudes 78°-84°N) for the DO series vs the CSR RL06.3 mascons (minus GRD and GAD_{avg}). Both series omit values in the newly-defined "land" mascons over Franz Josef Land.

2.3 Earthquake Model

Any oceanographer or sea level scientist who has tried to use GRACE/FO data in the northwestern Pacific or northern Indian Oceans has observed the enormous solid earth gravity signal caused by the two largest oceanic earthquakes which have occurred since GRACE's launch. The Andaman-Sumatra magnitude 9.2 earthquake occurred on 26 December 2004 and is easily visible (Fig. 5a) in any regional or global GRACE analysis (Han et al., 2006; Chen et al., 2007; Han et al., 2008; De Linage et al., 2009), as is the magnitude 9.0 Tōhoku, Japan earthquake (Fig. 5b) on 11 March 2011 (Cambiotti and Sabadini, 2012; Wang et al., 2012; Fuchs et al., 2013; Dai et al., 2014). Both megathrust earthquakes caused a shift in the solid earth gravity signal around the epicenter at the time of the earthquake (the co-seismic effect) and a long-term, near-linear drift after

https://doi.org/10.5194/essd-2025-718
Preprint. Discussion started: 15 January 2026

the earthquake (the post-seismic effect) which continues through this day (Fig. 5b). Various mascon solutions attempt to accommodate this highly localized gravity signal, but as Bonin et al. (2025) demonstrate, the pattern and magnitudes of the resulting mascon signal vary among GRACE/FO processing centers and is dependent on specific regularization and background model choices.

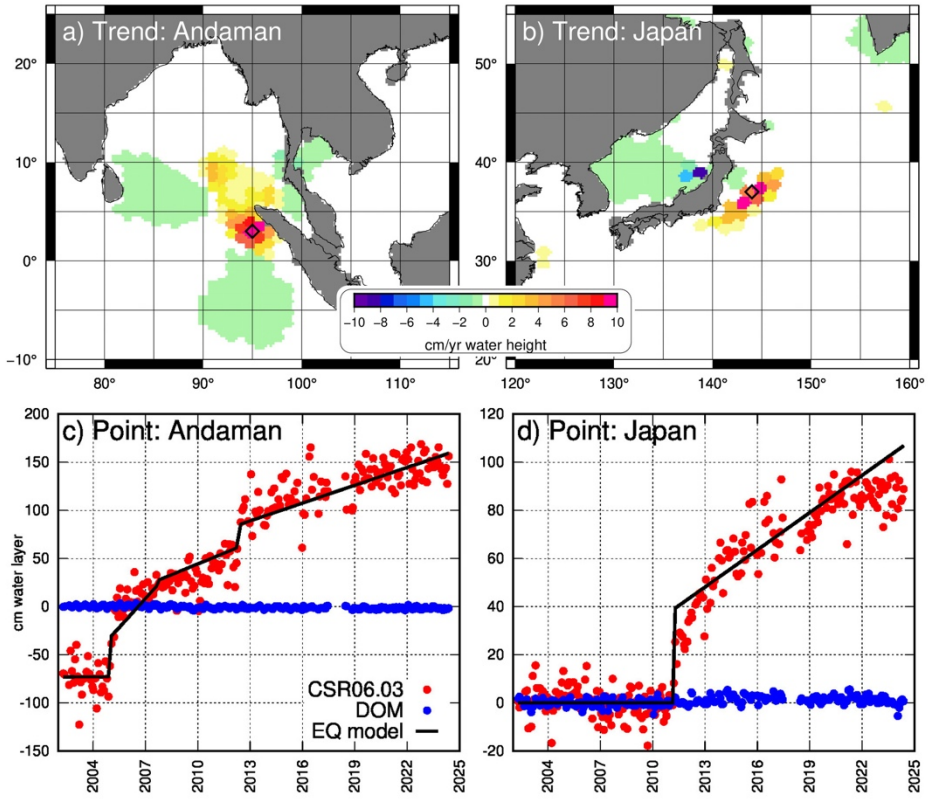

Figure 5: 2002-2025 Trend of CSR RL06.3 standard mascon series near (a) Andaman Bay and (b) Japan), plus timeseries (c, d) of a single mascon near each epicenter (locations shown as diamonds in a, b) for both CSR RL06.3 (red) and the DO mascons (blue). Timeseries of the earthquake model at the observed points is shown as the black line. (Global ocean means have been removed from RL06.3 each month, to approximate the removal of the GRD signal.)

For the Andaman-Sumatra earthquake, the CSR RL06.3 mascons observe a co-seismic jump of approximately 50 cm for the largest earthquake in 2004, with smaller jumps for subsequent earthquakes, along with up to 6 cm yr^{-1} post-seismic trends (after the last quake). The Tōhoku earthquake has a similar effect: about a 40 cm co-seismic bias near the epicenter, and a ~5 cm yr^{-1} trend in the decade afterwards. These gravity changes are an order of magnitude larger than observed sea level or ocean mass change (which is generally less than 0.3 cm yr^{-1} once barystatic-GRD is removed) and must be removed before the DO mascons can be considered useful for ocean dynamic studies in the region. We have estimated the non-oceanographic mass signals induced by the earthquakes using a localized principal component analysis (PCA) to isolate the two largest PCA modes,

https://doi.org/10.5194/essd-2025-718
Preprint. Discussion started: 15 January 2026

which explain ~98% of the local signal variance (Bonin et al, 2025; Pie and Bonin, 2025). The details of the methodology are beyond the scope of this paper but are described in Bonin et al. (2025). We demonstrate here that the recovered model matches the extreme mass signals quite well (Fig. 5c, d), and that after removing the model, the variance of the GRACE RL06.2DO mascons (and trends) is reduced to levels expected from oceanographic processes based on ocean mascons nearby (Fig. 6).

The earthquake model was estimated using the GRACE RL06.2 mascon data between April 2002 and February 2023. We extended the model's final linear fit from March 2023 to May 2024, which corresponds to the end of the RL06.2 series. We then included this earthquake model in the estimation background model as part of the Level-2 mascon processing stream used to estimate the new CSR RL06.2DO mascons. We did not simply subtract the model from the original mascons as a post-processing step, and do not recommend that the model we include in the dataset be used for this purpose on any other mascon data set. As Bonin et al (2025) demonstrated, by applying this earthquake model as a background model for the CSR mascon estimation processing, we are able to drastically tighten the constraints there. If one did not do this and simply removed the model from the GRACE RL06.2 mascons, there would be increased noise in the area of the earthquake because the RL06.2 constraints are relaxed to allow the earthquake signal into the proper mascons. For example, the standard deviation around the earthquake model at the epicenter of the Andaman-Sumatra earthquakes using the looser RL06.2 constraint is 8.5 cm, which is 4 times higher than for an ocean mascon far away from the epicenter (< 2 cm) (Fig. 6c, d). By applying the earthquake model as part of the processing stream, we improve the signal to noise ratio near the earthquake regions, resulting in reduced residual DO mascon noise levels over other mascon solutions, in addition to the obvious benefit of separating the solid earth signal from the desired ocean signal.

https://doi.org/10.5194/essd-2025-718
Preprint. Discussion started: 15 January 2026

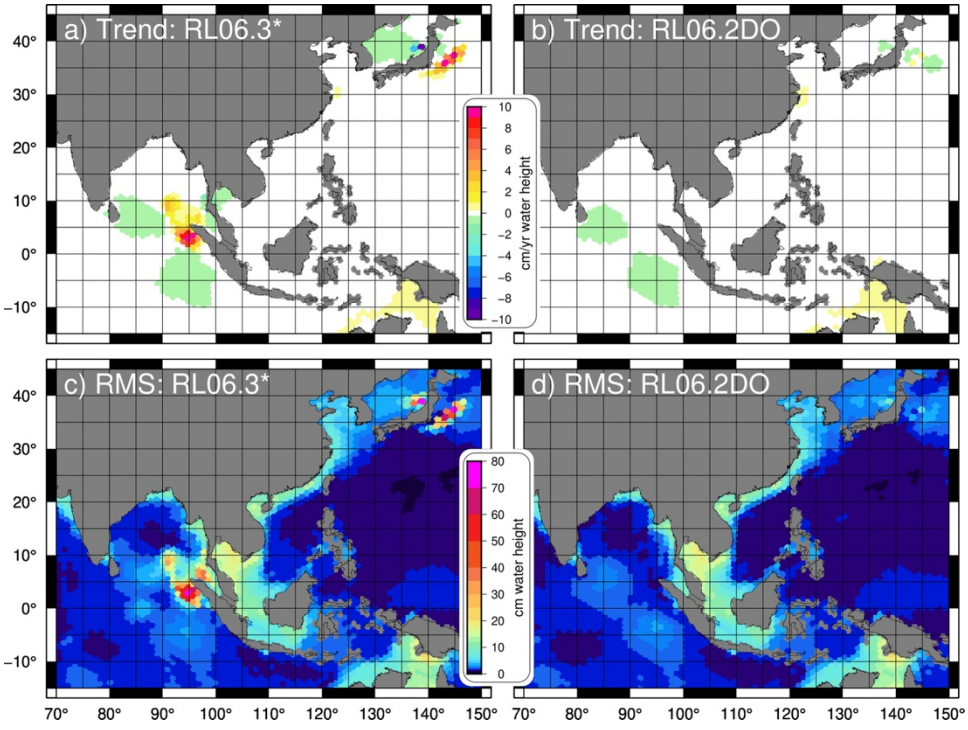

Figure 6: Trend and RMS of (a, c) the CSR RL06.3 mascons after the barystatic-GRD and GAD_{avg} have been removed, and (b, d) the DO mascons, from 2002-2023.

We provide the earthquake model used (Pie and Bonin, 2025) for users interested in the earthquake signal that was removed, and for those interested in restoring the earthquake model to obtain mascons less noisy in this region than the standard CSR RL06.2 mascons. However, our earthquake model grid should not be removed from mascons produced by other processing centers (e.g., Jet Propulsion Laboratory or Goddard Space Flight Center), or from gridded spherical harmonics, because these have different earthquake patterns that are dependent on their processing, background models, and regularizations used (Bonin et al., 2025).

2.4 GRD and Barystatic Ocean Mass Signals

There is a substantial time-variable exchange of mass between the oceans and the land/ice, on both a long-term and an annual-scale time frame (Fig. 7a), with the global average change in the ocean termed “barystatic” (Gregory et al., 2019). The associated gravitational, rotational, and deformational (GRD) effects caused by this mass motion creates large-scale, non-uniform patterns in ocean mass represented by the mascons (Fig. 7b,c) (e.g., Farrell & Clark, 1976). The combined barystatic-GRD signal will not cause dynamic ocean signals, since the timescale of the change is long enough for barotropic redistribution

https://doi.org/10.5194/essd-2025-718
Preprint. Discussion started: 15 January 2026

of the mass to occur and ocean pressure will reach equilibrium with no gradients (Ponte, 2006). The signal is largest near glaciated regions losing significant amounts of mass into the ocean (high negative trends in Fig. 7b around Greenland, Alaska, Patagonia, and West Antarctica), with a balancing far-field rise in ocean interiors. While trends are strongest near ice sheets, annual amplitudes are highest near large hydrological basins with strong seasonality that peaks at the same time as global ocean mass, such as the Bay of Bengal (Fig. 7c). Annual GRD signals near land may alternatively be suppressed, if the water storage in the basin peaks during the global ocean mass minimum (e.g., the Amazon) (Fig. 7c). There is an additional signal in the standard ocean mascons that arises from global ocean-area atmospheric pressure variations, seen as the average of the GAD product over the oceans (Fig. 7a, blue line). This signal is uniform over the ocean, and its inclusion means that the standard ocean mascons represent both internal ocean pressure variations (arising from geostrophic balance), GRD mass signals, and this atmospheric pressure variation. Because internal pressure variations should balance and be zero, global averages of the standard mascons reflect a combination of GRD and this atmospheric pressure signal (e.g., Chambers & Schröter, 2011).

Figure 7 shows only the estimated trend and annual amplitude, but we calculate the full barystatic-GRD signal over the same quasi-monthly period the mascons are computed over, based on the methods described in Tamisiea et al. (2010). This captures the full month-to-month variations and interannual changes as well. For this calculation, we use the DO mascons over land as an estimate of the hydrological+ice changes, which complements and drives the barystatic-GRD changes. Here, as in many GRD calculations, the contribution of dynamic ocean and atmospheric mass changes to the GRD estimate are not considered. In addition, because GRACE cannot independently estimate the spherical harmonic degree 1 variability of mass change, we simultaneously estimate it (similar to Sun et al., 2016a,b) to be consistent with the mascons and barystatic-GRD estimate. It must be noted that rotational signals have been removed from the GRACE data in the standard background models, and thus rotational components are not included in the barystatic-GRD estimate.

The monthly barystatic-GRD estimates are removed (along with the monthly GAD average over the ocean) to create the DO mascons. In doing this, we create a series of ocean mascons that have zero ocean-average mass change (Fig. 7a, black line), so that they will only show internal mass redistribution from ocean dynamics. Previous studies have attempted to estimate such grids for ocean applications (Song & Zlotnicki, 2008; Chambers & Willis, 2009; Landerer et al., 2015) by removing a uniform ocean mass signal (i.e., the time series shown in Fig. 7a applied uniformly for each grid cell). However, even after doing so, there are still small non-oceanographic artifacts left (Fig. 8b,d), particularly in the vicinity of Greenland, where the largest barystatic-GRD trend occurs. By estimating GRD, we avoid such artifacts (Fig. 8a,c).

https://doi.org/10.5194/essd-2025-718
Preprint. Discussion started: 15 January 2026

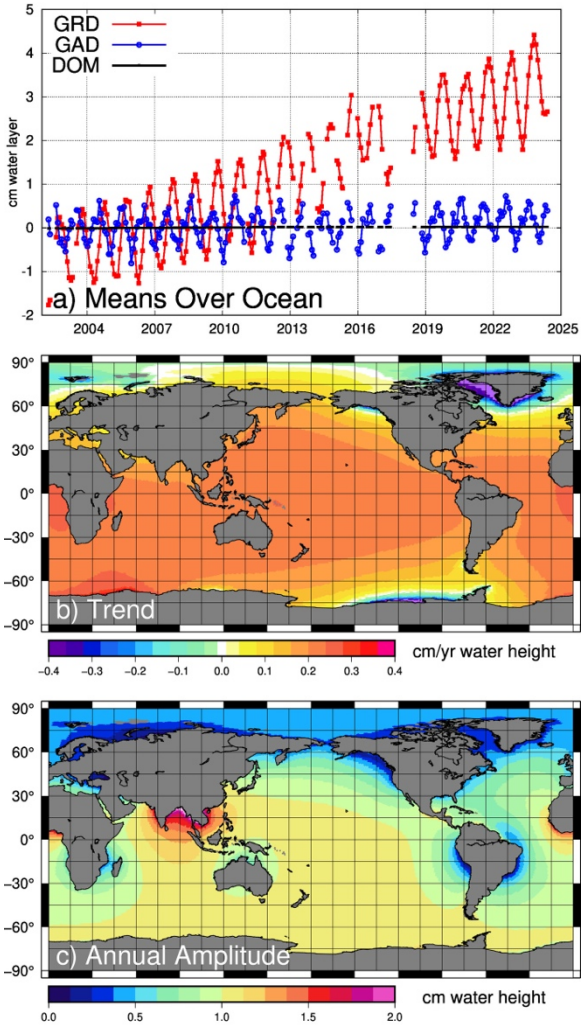

Figure 7: Mass exchange between the ocean and the rest of the globe, via: (a) mean signals over the global oceans, for the barystatic-GRD, the GAD, and the dynamic ocean mascons; and (b) trend and (c) annual amplitude distribution of the barystatic-GRD estimate.

https://doi.org/10.5194/essd-2025-718
Preprint. Discussion started: 15 January 2026

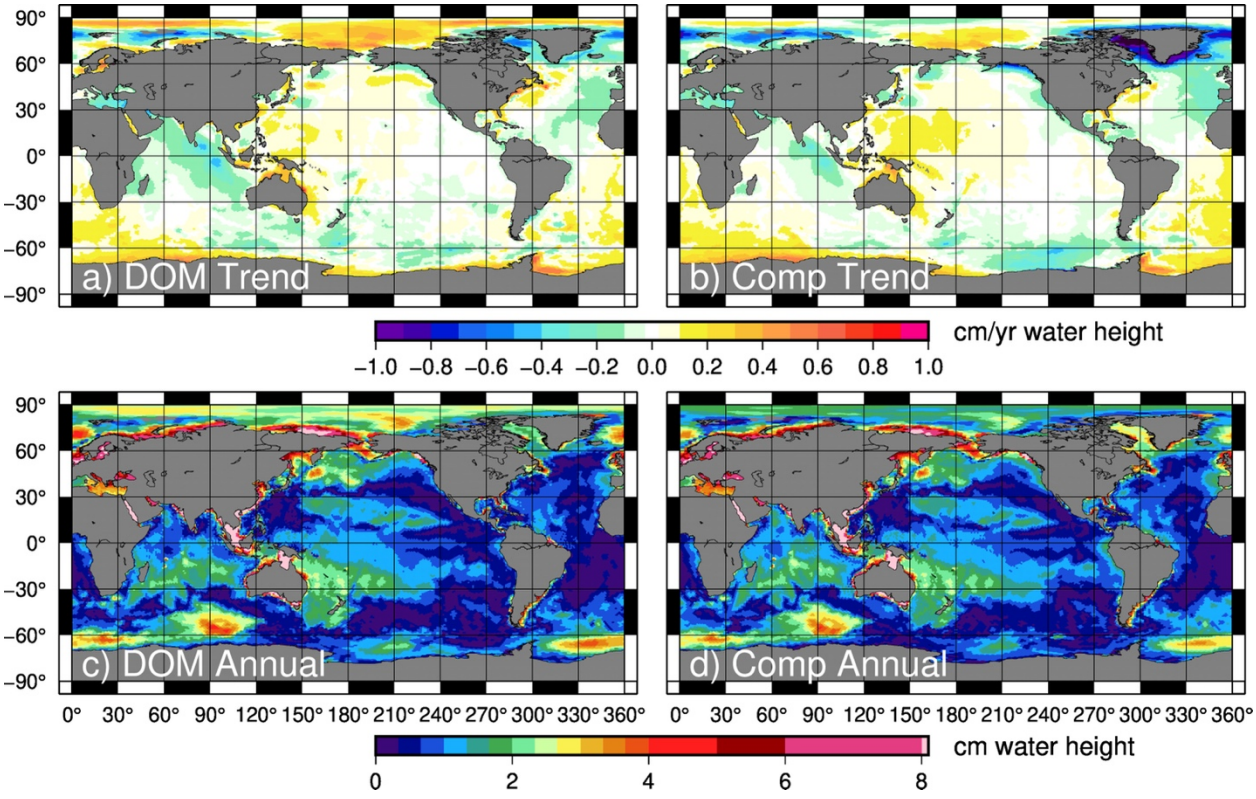

Figure 8: The trends (a,b) and annual amplitudes (c,d) of the DO mascons (left) compared to the case where a uniform global ocean average is removed rather than the GRD estimate (right).

The barystatic-GRD estimates affiliated with the dynamic ocean mascons are provided separately (Pie et al., 2025), in case users want to reapply them and/or remove their own GRD estimate.

3 Dynamic Ocean Mascon Statistics

We produced the dynamic ocean mascons using GRACE/FO data from April 2002 until May 2024, matching the full run of the RL06.2 data. The main product is provided with the earthquake model, barystatic-GRD effects, and the average of GAD over the ocean removed, such that the product is ready for oceanographic use. We have already demonstrated (Fig. 7a, black line) that total ocean mass remains constant in this series. We now show the linear trends (Fig. 9), annual amplitude (Fig. 10), and RMS of the residual with the bias, trend, annual, and semiannual removed (Fig. 11) for the most modern standard CSR mascon series (RL06.3) after the ocean mean has been removed each month, the DO mascons, and ocean bottom pressure from the ECCOv4r4 ocean state estimate (ECCO Consortium et al., 2021a, 2021b; Forget et al., 2015). Removing the monthly ocean mean from RL06.3 mimics the simple GRD-like removal that many ocean scientists have historically used (Song &

https://doi.org/10.5194/essd-2025-718
Preprint. Discussion started: 15 January 2026

Zlotnicki, 2008; Chambers & Willis, 2009; Landerer et al., 2015), such that the impact of RL06.2DO's more accurate barystatic-GRD estimation can be fairly evaluated. Please note that the ECCOv4r4 series includes a non-zero, time-varying global mean term to approximate water mass exchanges between land and ocean within the model. We subtract this monthly, uniform layer to make it more consistent with the DO mascons. Comparisons between ECCOv4r4 and the DO mascons are not appropriate without such a correction applied. Calculations are made from 2002-2017, the timespan when ECCOv4r4 and GRACE/FO overlap.

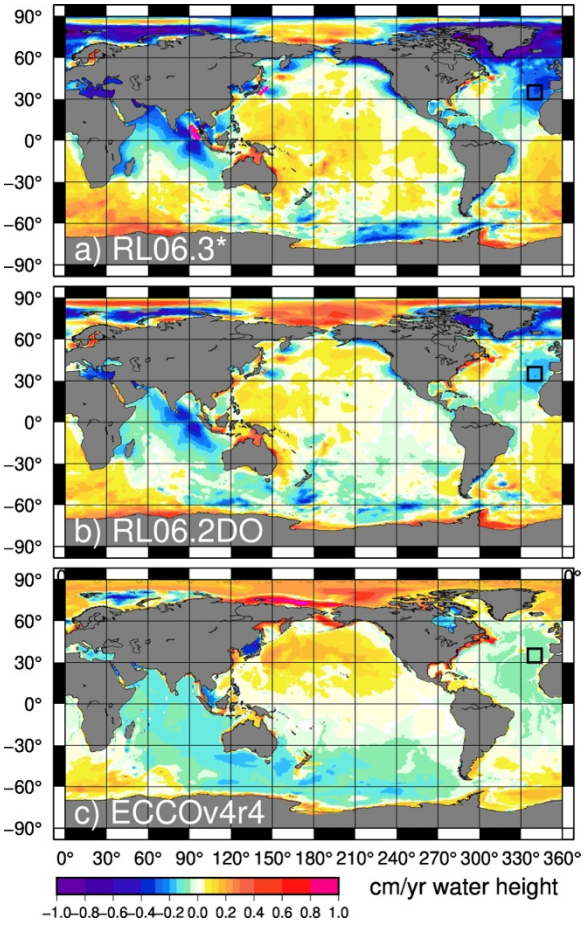

Figure 9: 2002-2017 trends from (a) CSR RL06.3 mascons after a uniform global ocean average is removed each month, (b) the DO mascons, and (c) the ECCOv4r4 model. Black box denotes the region averaged over to calculate the timeseries in Fig. 13.

There are substantial changes between the DO mascons and ocean-mean-removed RL06.3, particularly in terms of the Arctic-area linear trend, which is much closer to zero in the DO mascons. Trend reductions across the Pacific Ocean and differences in the annual amplitude across the Arctic Ocean are also visible. Most of this change is due to the removal of the barystatic-GRD signal, as opposed to the simpler technique of merely removing an ocean-wide mean for each month. Trend differences

https://doi.org/10.5194/essd-2025-718
Preprint. Discussion started: 15 January 2026

also occur near Franz Josef Land in the Arctic (see also Fig. 3), where the land/ocean mask and constraints were altered to more appropriately localize the land ice signal and prevent leakage into nearby ocean mascons. Around the earthquake regions, there are large local improvements caused by the removal of the model and the constraint tightening. While the model used in the DO processing has removed much of the variance caused by the earthquakes, some trends remain in the northern Indian Ocean and the northwestern Pacific Ocean, that are not entirely consistent with the larger-scale ocean trends in the area. Because they are centered on each earthquake epicenter, they are likely residual long-wavelength solid earth signals not removed by the earthquake model (Bonin et al., 2025). We recommend oceanographers working in these regions consider removing trends from the DO mascons and only use the residuals in their analysis.

By removing barystatic-GRD, the earthquake signal, and the effect of mean atmospheric pressure, we have created a series of mascons which reflects expected ocean dynamical variations, as evidenced in the ECCOv4r4 state estimate. For example, the DO mascons show mass losses in the Indian Ocean and Southern Ocean and rises in the South Atlantic, consistent with the ECCOv4r4 state estimate. The annual amplitudes (Fig. 10) are also similar and in expected areas consistent with seasonal ocean dynamics (e.g., Johnson & Chambers, 2013), such as seasonal changes in the Pacific subtropical gyres, the Indian Ocean circulation, and closed f/H contours in the Southern Ocean. The annual dominant fluctuation in the North Pacific, related to seasonal changes in wind stress curl (e.g., Chambers, 2011) is also clearer in the DO mascons.

https://doi.org/10.5194/essd-2025-718
Preprint. Discussion started: 15 January 2026

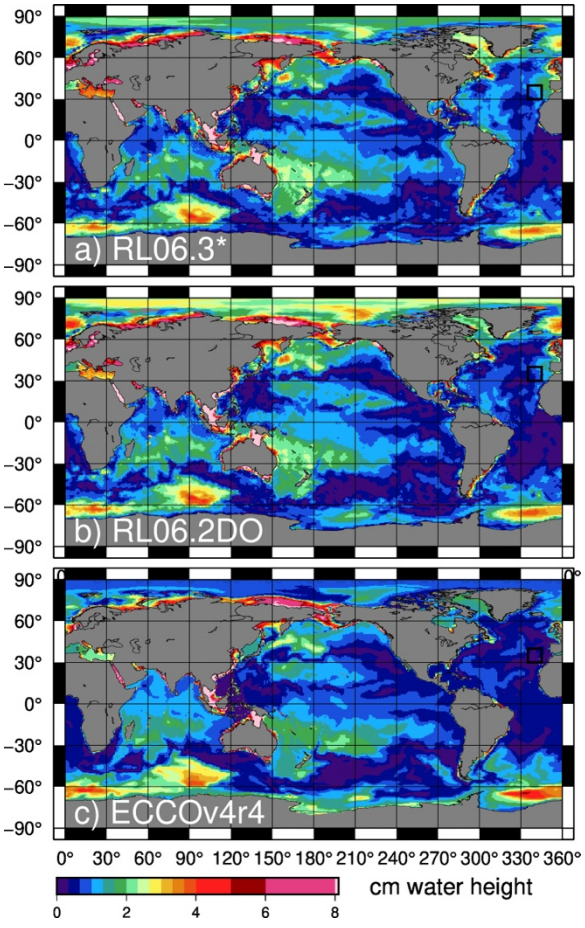

Figure 10: 2002-2017 annual amplitudes from (a) CSR RL06.3 mascons after a uniform global ocean average is removed each month, (b) the DO mascons, and (c) the ECCOv4r4 model.

Non-seasonal variability in the DO mascons has similar magnitude and locations as that seen in ECCOv4r4 (Fig. 11), with the largest variability at high latitudes and lower values at the equator. Generally, the equatorial variance is a good measure of the noise floor in the DO mascons. The level of high-frequency (non-annual) variability there should be quite small, with standard deviation well below 1 cm. Average ECCOv4r4 equatorial RMS residuals are ~0.6 cm (see Fig. 11b), suggesting the approximate RMS of the expected signal. The DO mascons have a value ~0.4 cm higher (average values ~1 cm). Using the root sum of squares, this suggests ~0.8 cm RMS is a reasonable approximation of the month-to-month uncertainty in the DO mascons.

https://doi.org/10.5194/essd-2025-718
Preprint. Discussion started: 15 January 2026

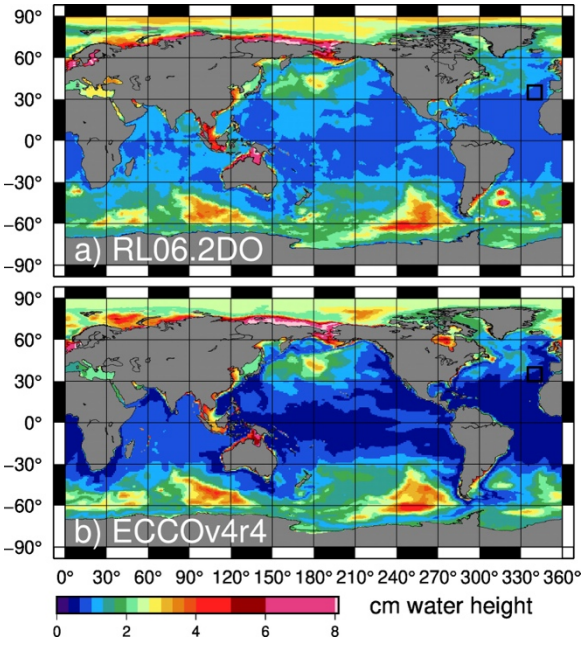

Figure 11: 2002-2017 residual RMS from (a) the DO mascons, and (b) the ECCOv4r4 model. Trend, annual, and semiannual effects have been removed.

There are several notable areas where the DO mascons capture signals that are not represented in the ECCOv4r4 model. One occurs in near the North Pole, which has previously been shown to have large seasonal mass variations and compare well between pressure gauges and early GRACE data (Peralta-Ferriz and Morison, 2010; Peralta-Ferriz et al., 2016). The DO mascons have a larger annual amplitude there compared to ECCOv4r4. The ECCOv4r4 state estimate also peaks in June and decays rapidly thereafter, while the DO monthly climatological signal ramps up until June but remains high from then through October (Fig. 12). Considering the limited observations that ECCOv4r4 runs can assimilate in the Arctic (compared to the rest of the ocean) and the fact that previous studies have shown strong agreement between bottom pressure recorders and GRACE, we assume this reflects a true ocean signal observed in the DO mascons that is not captured by ECCOv4r4.

https://doi.org/10.5194/essd-2025-718
Preprint. Discussion started: 15 January 2026

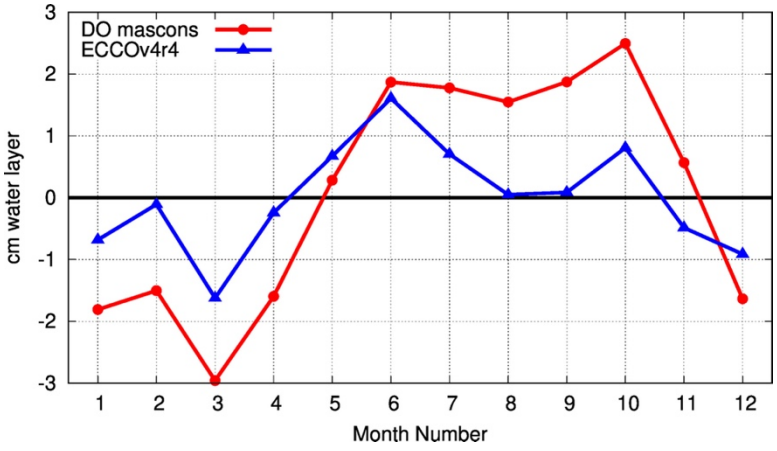

Figure 12: Differences in monthly climatology of average within 5° longitude of the north pole.

One signal which we know is seen in the DO mascons and not ECCOv4r4 is the high variability in the Argentine basin east of Brazil (Fig. 11), which has a known, sub-annual barotropic variation (Fu, 2007; Hughes et al., 2007; Yu et al., 2018). It is not present in ECCOv4r4 (or the ocean dealiasing product used for GRACE/FO processing), but is recovered by GRACE/FO mascons, both the original and the DO versions.

The DO mascons have significant non-zero negative trends east and west of Greenland (Fig. 9), especially in Baffin Bay. These are not present in ECCOv4r4. While the removal of GRD reduces these trends from the original mascons (Fig. 9b vs 9a), they are still substantial and generally in the same direction as ice mass loss from Greenland. Because ECCOv4r4 does not suggest significant bottom pressure trends in these regions, and since the regions are bordered by large ice mass losses on both sides, we suspect these signals are due to residual leakage and suggest caution when using the DO mascons near Greenland.

The final area with a significant difference is in the NE Atlantic, where the DO mascons suggest a large (-1.8 mm yr^{-1}) drop in mass/bottom pressure, while ECCOv4r4 suggests a much smaller (-0.7 mm yr^{-1}) change (Fig. 13). This signal is not unique to the DO mascons. It appears as an even larger trend in the standard mascons (Fig. 9a), as well as mascons and gridded spherical harmonics from other processing centers. This indicates it is probably a real gravity signal that the GRACE/FO observations must accommodate, not some sort of error due to (for example) a specific version of mascon regularization. However, it is difficult to theorize an ocean dynamic signal which could cause such a large linear trend over the course of the entire GRACE/FO mission. While the lower limb of the Atlantic Meridional Overturning Circulation (AMOC) does cause bottom pressure variations (Bingham and Hughes, 2006; Elipot et al., 2014; Landerer et al., 2015; Frajka-Williams et al., 2018), ocean mass transport on the western side of the Atlantic is an order of magnitude larger than on the eastern side. Moreover, a large drop in pressure on the eastern side would also suggest a large increase in the southward flow of the AMOC

https://doi.org/10.5194/essd-2025-718
Preprint. Discussion started: 15 January 2026

lower limb, which has not been observed in any of the instrumented arrays measuring the upper limb transport across the Atlantic (Smeed et al., 2018; Johns et al., 2023; Volkov et al., 2024). These studies show either a small decrease in upper limb transport across 26.5°N latitude or no decrease, which is inconsistent with the bottom pressure signature in the GRACE/FO mascons north of the latitude. A difference in the sign of change in the transport between the lower and upper limbs of AMOC across 26.5°N is impossible from mass conservation, as it would cause a drop in sea level over the entire North Atlantic of several meters, which has never been observed.

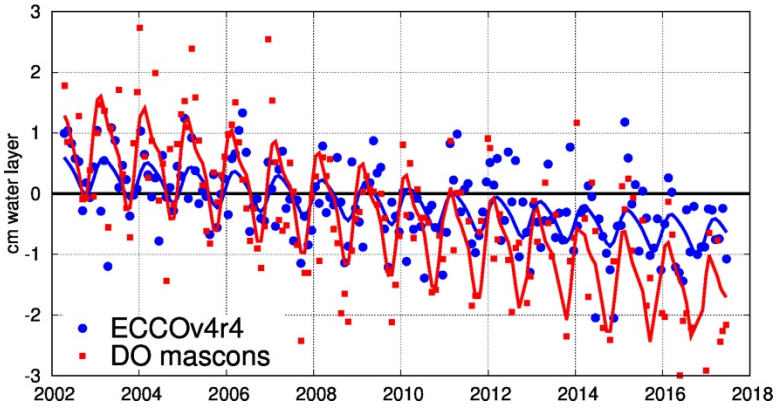

Figure 13: Average mass change (in terms of water height) in the region of the northeastern Atlantic drawn in Figure 9.

Thus, we conclude that the bottom pressure trend observed in all GRACE (and presumably GRACE-FO) data in the northeast Atlantic cannot be oceanographic in nature. It is beyond the scope of this study to determine what could be responsible for the signal, but we suspect it is more likely a solid earth gravity signal that deserves further investigation. We would recommend any studies of AMOC transport based on east-west gradients of bottom pressure across the Atlantic using the GRACE/FO data (e.g., Landerer et al., 2015) to continue to remove local trends and only consider non-linear transport variations.

4 Conclusions

The dynamic ocean mascons are available at the Texas Data Depository (Pie et al., 2025). The barystatic-GRD estimate (dataset: CSR_GRACE_GRACE-FO_RL06.2DO_Mascons_GRD-component.nc) and earthquake model (dataset: CSR_GRACE_GRACE-FO_RL06.2DO_Mascons_EQ-component.nc) are also available, if users care to investigate those or restore them and remove their own estimates. The new mascons extend from the start of GRACE (April 2002) through the end of the CSR RL06.2 series (May 2024), making a total of 22 years of data. Gaps exist for those months where data does not exist in other GRACE/FO series, including the year-long gap between June 2017 and June 2018, between the two missions.

https://doi.org/10.5194/essd-2025-718
Preprint. Discussion started: 15 January 2026

505

The dynamic ocean mascons (with the removed components added back) are very similar to the CSR RL06.2 (and RL06.3) mascons they were based on, except for changes in the earthquake and Franz Josef Land areas, near polar coastlines, and in the geocenter term (a smaller but global effect). The primary benefit of the series is ease of use: oceanographers do not need to be experts in GRACE/FO processing to use this data for research. Like other mascon series, the data is in a simple gridded
510 format that does not require spherical harmonic knowledge to read. The gravity signals which are caused by ocean dynamics have been partitioned from the non-ocean-caused gravity signals, properly accounting for mass variations caused by mass exchange with land, barystatic-GRD, the solid earth motion due to four large oceanic earthquakes, and the force of global atmospheric pressure. Because most non-oceanographic signals have already been removed, this product is expected to be an easy starting point for oceanographic use.

515

The dynamic ocean mascons are designed to be comparable to ocean models (once conservation of mass is taken into account within the model). We remind users that this is a measure of dynamic ocean mass change, not a measure of bottom pressure. The dynamic ocean mascons should not be compared to ocean bottom pressure recorders or models of ocean bottom pressure. They also should not be directly compared to any ocean model with non-zero mean mass change across the ocean (including
520 the standard ECCOv4r4 release, unless you also remove the monthly ocean means). The dynamic ocean mascons, however, are useful for comparisons to mass-conserving models, for assimilation into ocean models, and for comparisons with or estimates of dynamic ocean signals.

5 Data availability

525

The standard CSR RL0602 mascon series that this work was based upon has since been superseded by the very similar CSR RL0603 data. Those mascon series are freely available at https://www2.csr.utexas.edu/grace/RL06_mascons.html (last access 3 Nov. 2025).

530 The resulting dynamic ocean mascons are available at the Texas Data Depository (Pie et al., 2025) at https://doi.org/10.18738/T8/3VUPEW. The barystatic-GRD estimate (dataset: "CSR_GRACE_GRACE-FO_RL06.2DO_Mascons_GRD-component.nc") and earthquake model (dataset: "CSR_GRACE_GRACE-FO_RL06.2DO_Mascons_EQ-component.nc") are also available there as separate files.

535

6 Author Contribution

https://doi.org/10.5194/essd-2025-718
Preprint. Discussion started: 15 January 2026

The various mascon series, including the final DO mascons, were created by Pie, with the aid and structural support of Tamisiea and Save. The barystatic-GRD series was developed, created, and applied by Tamisiea. The earthquake series was developed and created by Bonin and Pie. Constraint alteration tests were run by Pie, with analysis of their results done by all co-authors. All members of the team aided in the final analysis of the DO mascons, with Chambers acting as oceanographic expert. Bonin prepared the manuscript with contributions from all co-authors.

7 Acknowledgments

The authors acknowledge the Texas Advanced Computing Center (TACC) at The University of Texas at Austin for providing computational resources that have contributed to the research results reported within this paper. URL: http://www.tacc.utexas.edu.

8 Competing Interests

The authors declare that they have no conflict of interest.

References

Bergmann, I. and Dobslaw, H.: Short-term transport variability of the Antarctic Circumpolar Current from satellite gravity observations, J Geophys Res Oceans, 117, https://doi.org/10.1029/2012JC007872, 2012.

Bingham, R. J. and Hughes, C. W.: Observing seasonal bottom pressure variability in the North Pacific with GRACE, Geophys Res Lett, 33, https://doi.org/10.1029/2005GL025489, 2006.

Boening, C., Willis, J. K., Landerer, F. W., Nerem, R. S., and Fasullo, J.: The 2011 la Nia: So strong, the oceans fell, Geophys Res Lett, 39, https://doi.org/10.1029/2012GL053055, 2012.

Bonin, J. A., Pie, N., Chambers, D. P., Tamisiea, M. E., and Save, H.: Detection and Modeling of Earthquake Signals in GRACE/GRACE-FO Mascons, in review for final publication in Earth Space Science, currently viewable in Authorea, doi:10.22541/au.173879122.22467584/v1, 2025.

Cambiotti, G. and Sabadini, R.: A source model for the great 2011 Tohoku earthquake (M w=9.1) from inversion of GRACE gravity data, Earth Planet Sci Lett, 335–336, 72–79, https://doi.org/10.1016/j.epsl.2012.05.002, 2012.

https://doi.org/10.5194/essd-2025-718
Preprint. Discussion started: 15 January 2026

570 Cazenave, A., Hamlington, B., Horwath, M., Barletta, V. R., Benveniste, J., Chambers, D., Döll, P., Hogg, A. E., Legeais, J. F., Merrifield, M., Meyssignac, B., Mitchum, G., Nerem, S., Pail, R., Palanisamy, H., Paul, F., von Schuckmann, K., and Thompson, P.: Observational requirements for long-term monitoring of the global mean sea level and its components over the altimetry era, Front Mar Sci, 6, https://doi.org/10.3389/fmars.2019.00582, 2019.

Chambers, D. P.: Observing seasonal steric sea level variations with GRACE and satellite altimetry, J Geophys Res Oceans, 575 111, https://doi.org/10.1029/2005JC002914, 2006.

Chambers, D. P.: ENSO-correlated fluctuations in ocean bottom pressure and wind-stress curl in the North Pacific, Ocean Science, 7, 685–692, https://doi.org/10.5194/os-7-685-2011, 2011.

Chambers, D. P. and Schröter, J.: Measuring ocean mass variability from satellite gravimetry, https://doi.org/10.1016/j.jog.2011.04.004, December 2011.

580 Chambers, D. P. and Willis, J. K.: Analysis of large-scale ocean bottom pressure variability in the North Pacific, J Geophys Res Oceans, 113, https://doi.org/10.1029/2008JC004930, 2008.

Chambers, D. P. and Willis, J. K.: Low-frequency exchange of mass between ocean basins, J Geophys Res Oceans, 114, https://doi.org/10.1029/2009JC005518, 2009.

Chambers, D. P., Cazenave, A., Champollion, N., Dieng, H., Llovel, W., Forsberg, R., von Schuckmann, K., and Wada, Y.: 585 Evaluation of the Global Mean Sea Level Budget between 1993 and 2014, https://doi.org/10.1007/s10712-016-9381-3, 1 January 2017.

Chao, B. F. and Liau, J. R.: Gravity Changes Due to Large Earthquakes Detected in GRACE Satellite Data via Empirical Orthogonal Function Analysis, J Geophys Res Solid Earth, 124, 3024–3035, https://doi.org/10.1029/2018JB016862, 2019.

Chen, J. L., Wilson, C. R., Tapley, B. D., and Grand, S.: GRACE detects coseismic and postseismic deformation from the 590 Sumatra-Andaman earthquake, Geophys Res Lett, 34, https://doi.org/10.1029/2007GL030356, 2007.

Cheng, X., Li, L., Du, Y., Wang, J., and Huang, R. X.: Mass-induced sea level change in the northwestern North Pacific and its contribution to total sea level change, Geophys Res Lett, 40, 3975–3980, https://doi.org/10.1002/grl.50748, 2013.

Ciracì, E., Velicogna, I., and Swenson, S.: Continuity of the Mass Loss of the World's Glaciers and Ice Caps From the GRACE and GRACE Follow-On Missions, Geophys Res Lett, 47, https://doi.org/10.1029/2019GL086926, 2020.

595 Dai, C., Shum, C. K., Wang, R., Wang, L., Guo, J., Shang, K., and Tapley, B.: Improved constraints on seismic source parameters of the 2011 Tohoku earthquake from GRACE gravity and gravity gradient changes, Geophys Res Lett, 41, 1929–1936, https://doi.org/10.1002/2013GL059178, 2014.

Ditmar, P.: Conversion of time-varying Stokes coefficients into mass anomalies at the Earth's surface considering the Earth's oblateness, J Geod, 92, 1401–1412, https://doi.org/10.1007/s00190-018-1128-0, 2018.

600 Dobslaw, H., Bergmann-Wolf, I., Dill, R., Poropat, L., Thomas, M., Dahle, C., Esselborn, S., König, R., and Flechtner, F.: A new high-resolution model of non-tidal atmosphere and ocean mass variability for de-aliasing of satellite gravity observations: AOD1B RL06, Geophys J Int, 211, 263–269, https://doi.org/10.1093/GJI/GGX302, 2017.

https://doi.org/10.5194/essd-2025-718
Preprint. Discussion started: 15 January 2026

ECCO Consortium, Fukumori, I., Wang, O., Fenty, I., Forget, G., Heimbach, P., and Ponte, R. M.: ECCO Ocean Bottom Pressure - Monthly Mean 0.5 Degree (Version 4 Release 4 B), https://doi.org/10.5067/ECTSM-MSL44, 2021a.

ECCO Consortium, Fukumori, I., Wang, O., Fenty, I., Forget, G., Heimbach, P., and Ponte, R. M.: Synopsis of the ECCO Central Production Global Ocean and Sea-Ice State Estimate, Version 4 Release 4, 2021b.

Elipot, S., Frajka-Williams, E., Hughes, C. W., and Willis, J. K.: The observed North Atlantic meridional overturning circulation: Its meridional coherence and ocean bottom pressure, J Phys Oceanogr, 44, 517–537, https://doi.org/10.1175/JPO-D-13-026.1, 2014.

Farrell, W. E. and Clark, J. A.: On Postglacial Sea Level, Geophysical Journal of the Royal Astronomical Society, 46, 647–667, 1976.

Feng, G., Jin, S., and Reales, J. M. S.: Antarctic circumpolar current from satellite gravimetric models ITG-GRACE2010, GOCE-TIM3 and satellite altimetry, J Geodyn, 72, 72–80, https://doi.org/10.1016/j.jog.2013.08.005, 2013.

Forget, G., Campin, J. M., Heimbach, P., Hill, C. N., Ponte, R. M., and Wunsch, C.: ECCO version 4: An integrated framework for non-linear inverse modeling and global ocean state estimation, Geosci Model Dev, 8, 3071–3104, https://doi.org/10.5194/gmd-8-3071-2015, 2015.

Frajka-Williams, E., Lankhorst, M., Koelling, J., and Send, U.: Coherent circulation changes in the deep north atlantic from 16°N and 26°N transport arrays, J Geophys Res Oceans, 123, 3427–3443, https://doi.org/10.1029/2018JC013949, 2018.

Fu, L. L.: Interaction of mesoscale variability with large-scale waves in the Argentine Basin, J Phys Oceanogr, 37, 787–793, https://doi.org/10.1175/JPO2991.1, 2007.

Fuchs, M. J., Bouman, J., Broerse, T., Visser, P., and Vermeersen, B.: Observing coseismic gravity change from the Japan Tohoku-Oki 2011 earthquake with GOCE gravity gradiometry, J Geophys Res Solid Earth, 118, 5712–5721, https://doi.org/10.1002/jgrb.50381, 2013.

Gregory, J. M., Griffies, S. M., Hughes, C. W., Lowe, J. A., Church, J. A., Fukimori, I., Gomez, N., Kopp, R. E., Landerer, F., Cozannet, G. Le, Ponte, R. M., Stammer, D., Tamisiea, M. E., and van de Wal, R. S. W.: Concepts and Terminology for Sea Level: Mean, Variability and Change, Both Local and Global, https://doi.org/10.1007/s10712-019-09525-z, 1 November 2019.

Han, S. C., Sauber, J., Luthcke, S. B., Ji, C., and Pollitz., F. F.: Implications of postseismic gravity change following the great 2004 Sumatra-Andaman earthquake from the regional harmonic analysis of GRACE intersatellite tracking data, J Geophys Res Solid Earth, 113, https://doi.org/10.1029/2008JB005705, 2008.

Han, S.-C., Shum, C. K., Bevis, M., Ji, C., and Kuo, C.-Y.: Crustal Dilatation Observed by GRACE after the 2004 Sumatra-Andaman Earthquake, Science (1979), 313, 658–662, https://doi.org/10.1029/2004GL021922, 2006.

Hughes, C. W., Stepanov, V. N., Fu, L. L., Barnier, B., and Hargreaves, G. W.: Three forms of variability in Argentine Basin ocean bottom pressure, J Geophys Res Oceans, 112, https://doi.org/10.1029/2006JC003679, 2007.

Jacob, T., Wahr, J., Pfeffer, W. T., and Swenson, S.: Recent contributions of glaciers and ice caps to sea level rise, Nature, 482, 514–518, https://doi.org/10.1038/nature10847, 2012.

https://doi.org/10.5194/essd-2025-718
Preprint. Discussion started: 15 January 2026

Jeffree, J., Hogg, A. M. C., Morrison, A. K., Solodoch, A., Stewart, A. L., and McGirr, R.: GRACE Satellite Observations of Antarctic Bottom Water Transport Variability, J Geophys Res Oceans, 129, https://doi.org/10.1029/2024JC020990, 2024.

Johns, W. E., Elipot, S., Smeed, D. A., Moat, B., King, B., Volkov, D. L., and Smith, R. H.: Towards two decades of Atlantic Ocean mass and heat transports at 26.5° N, Philosophical Transactions of the Royal Society A: Mathematical, Physical and Engineering Sciences, 381, https://doi.org/10.1098/rsta.2022.0188, 2023.

Johnson, G. C. and Chambers, D. P.: Ocean bottom pressure seasonal cycles and decadal trends from GRACE Release-05: Ocean circulation implications, J Geophys Res Oceans, 118, 4228–4240, https://doi.org/10.1002/jgrc.20307, 2013.

Landerer, F. W., Wiese, D. N., Bentel, K., Boening, C., and Watkins, M. M.: North Atlantic meridional overturning circulation variations from GRACE ocean bottom pressure anomalies, Geophys Res Lett, 42, 8114–8121, https://doi.org/10.1002/2015GL065730, 2015.

De Linage, C., Rivera, L., Hinderer, J., Boy, J. P., Rogister, Y., Lambotte, S., and Biancale, R.: Separation of coseismic and postseismic gravity changes for the 2004 Sumatra - Andaman earthquake from 4.6 yr of GRACE observations and modelling of the coseismic change by normal-modes summation, Geophys J Int, 176, 695–714, https://doi.org/10.1111/j.1365-246X.2008.04025.x, 2009.

Loomis, B. D., Luthcke, S. B., and Sabaka, T. J.: Regularization and error characterization of GRACE mascons, J Geod, 93, 1381–1398, https://doi.org/10.1007/s00190-019-01252-y, 2019.

Loomis, B. D., Rachlin, K. E., Wiese, D. N., Landerer, F. W., and Luthcke, S. B.: Replacing GRACE/GRACE-FO C30 With Satellite Laser Ranging: Impacts on Antarctic Ice Sheet Mass Change, Geophys Res Lett, 47, https://doi.org/10.1029/2019GL085488, 2020.

Makowski, J. K., Chambers, D. P., and Bonin, J. A.: Using ocean bottom pressure from the gravity recovery and climate experiment (GRACE) to estimate transport variability in the southern Indian Ocean, J Geophys Res Oceans, 120, https://doi.org/10.1002/2014JC010575, 2015.

Mazloff, M. R. and Boening, C.: Rapid variability of Antarctic Bottom Water transport into the Pacific Ocean inferred from GRACE, Geophys Res Lett, 43, 3822–3829, https://doi.org/10.1002/2016GL068474, 2016.

Peltier, R. W., Argus, D. F., and Drummond, R.: Comment on "An assessment of the ICE6G_C(VM5a) glacial isostatic adjustment model" by Purcell et al., J Geophys Res Solid Earth, 121, 2019–2028, https://doi.org/10.1002/2016JB013844, 2017.

Peralta-Ferriz, C. and Morison, J.: Understanding the annual cycle of the Arctic Ocean bottom pressure, Geophys Res Lett, 37, https://doi.org/10.1029/2010GL042827, 2010.

Peralta-Ferriz, C., Morison, J. H., and Wallace, J. M.: Proxy representation of Arctic ocean bottom pressure variability: Bridging gaps in GRACE observations, Geophys Res Lett, 43, 9183–9191, https://doi.org/10.1002/2016GL070137, 2016.

Pie, N. and Bonin, J.: CSR GRACE and GRACE-FO Ocean Mascons RL06.2EQ, Texas Data Repository, V1, https://doi.org/10.18738/T8/ZE7DUD, 2025.

https://doi.org/10.5194/essd-2025-718
Preprint. Discussion started: 15 January 2026

Pie, N., Bonin, J., Tamisiea, M., Chambers, D., and Save, H.: CSR GRACE & GRACE-FO Dynamic Ocean Mascons RL06.2DO, Texas Data Repository, V2, https://doi.org/10.18738/T8/3VUPEW, 2024.

Ponte, R. M.: Oceanic Response to Surface Loading Effects Neglected in Volume-Conserving Models, 2006.

Rodell, M. and Reager, J. T.: Water cycle science enabled by the GRACE and GRACE-FO satellite missions, Nature Water, 1, 47–59, https://doi.org/10.1038/s44221-022-00005-0, 2023.

Save, H.: CSR GRACE and GRACE-FO RL06 Mascon Solutions v02, https://doi.org/10.15781/cgq9-nh24, 2020.

Save, H., Bettadpur, S., and Tapley, B. D.: Reducing errors in the GRACE gravity solutions using regularization, J Geod, 86, 695–711, https://doi.org/10.1007/s00190-012-0548-5, 2012.

Save, H., Bettadpur, S., and Tapley, B. D.: High-resolution CSR GRACE RL05 mascons, J Geophys Res Solid Earth, 121, 7547–7569, https://doi.org/10.1002/2016JB013007, 2016.

Schmidt, L. S., Schuler, T. V., Westermann, S., and Dürig, T.: The climatic mass balance of glaciers on Franz Josef Land and Novaya Zemlya, 1991-2022, Journal of Glaciology, https://doi.org/10.1017/jog.2024.97, 2025.

Smeed, D. A., Josey, S. A., Beaulieu, C., Johns, W. E., Moat, B. I., Frajka-Williams, E., Rayner, D., Meinen, C. S., Baringer, M. O., Bryden, H. L., and McCarthy, G. D.: The North Atlantic Ocean Is in a State of Reduced Overturning, Geophys Res Lett, 45, 1527–1533, https://doi.org/10.1002/2017GL076350, 2018.

Song, Y. T. and Zlotnicki, V.: Subpolar ocean bottom pressure oscillation and its links to the tropical ENSO, in: International Journal of Remote Sensing, 6091–6107, https://doi.org/10.1080/01431160802175538, 2008.

Sun, Y., Ditmar, P., and Riva, R.: Observed changes in the Earth's dynamic oblateness from GRACE data and geophysical models, J Geod, 90, 81–89, https://doi.org/10.1007/s00190-015-0852-y, 2016a.

Sun, Y., Riva, R., and Ditmar, P.: Optimizing estimates of annual variations and trends in geocenter motion and J2 from a combination of GRACE data and geophysical models, J Geophys Res Solid Earth, 121, 8352–8370, https://doi.org/10.1002/2016JB013073, 2016b.

Swenson, S., Chambers, D., and Wahr, J.: Estimating geocenter variations from a combination of GRACE and ocean model output, J Geophys Res Solid Earth, 113, https://doi.org/10.1029/2007JB005338, 2008.

Tamisiea, M. E., Hill, E. M., Ponte, R. M., Davis, J. L., Velicogna, I., and Vinogradova, N. T.: Impact of self-attraction and loading on the annual cycle in sea level, J Geophys Res Oceans, 115, https://doi.org/10.1029/2009JC005687, 2010.

Tapley, B. D., Chambers, D. P., Bettadpur, S., and Ries, J. C.: Large scale ocean circulation from the GRACE GGM01 Geoid, Geophys Res Lett, 30, https://doi.org/10.1029/2003GL018622, 2003.

Tapley, B. D., Watkins, M. M., Flechtner, F., Reigber, C., Bettadpur, S., Rodell, M., Sasgen, I., Famiglietti, J. S., Landerer, F. W., Chambers, D. P., Reager, J. T., Gardner, A. S., Save, H., Ivins, E. R., Swenson, S. C., Boening, C., Dahle, C., Wiese, D. N., Dobslaw, H., Tamisiea, M. E., and Velicogna, I.: Contributions of GRACE to understanding climate change, https://doi.org/10.1038/s41558-019-0456-2, 1 May 2019.

https://doi.org/10.5194/essd-2025-718
Preprint. Discussion started: 15 January 2026

Velicogna, I., Mohajerani, Y., Geruo, A., Landerer, F., Mouginot, J., Noel, B., Rignot, E., Sutterley, T., van den Broeke, M., van Wessem, M., and Wiese, D.: Continuity of Ice Sheet Mass Loss in Greenland and Antarctica From the GRACE and GRACE Follow-On Missions, Geophys Res Lett, 47, https://doi.org/10.1029/2020GL087291, 2020.

Volkov, D. L., Smith, R. H., Garcia, R. F., Smeed, D. A., Moat, B. I., Johns, W. E., and Baringer, M. O.: Florida Current transport observations reveal four decades of steady state, Nature Communications , 15, https://doi.org/10.1038/s41467-024-51879-5, 2024.

Wahr, J., Molenaar, M., and Bryan, F.: Time variability of the Earth's gravity field' Hydrological and oceanic effects and their possible detection using GRACE, JOURNAL OF GEOPHYSICAL RESEARCH, 1998.

Wang, L., Shum, C. K., Simons, F. J., Tapley, B., and Dai, C.: Coseismic and postseismic deformation of the 2011 tohoku-oki earthquake constrained by GRACE gravimetry, Geophys Res Lett, 39, https://doi.org/10.1029/2012GL051104, 2012.

Watkins, M. M., Wiese, D. N., Yuan, D. N., Boening, C., and Landerer, F. W.: Improved methods for observing Earth's time variable mass distribution with GRACE using spherical cap mascons, J Geophys Res Solid Earth, 120, 2648–2671, https://doi.org/10.1002/2014JB011547, 2015.

Wiese, D. N., Landerer, F. W., and Watkins, M. M.: Quantifying and reducing leakage errors in the JPL RL05M GRACE mascon solution, Water Resour Res, 52, 7490–7502, https://doi.org/10.1002/2016WR019344, 2016.

Yu, Y., Chao, B. F., García-García, D., and Luo, Z.: Variations of the Argentine Gyre Observed in the GRACE Time-Variable Gravity and Ocean Altimetry Measurements, J Geophys Res Oceans, 123, 5375–5387, https://doi.org/10.1029/2018JC014189, 2018.

Zheng, W., Pritchard, M. E., Willis, M. J., Tepes, P., Gourmelen, N., Benham, T. J., and Dowdeswell, J. A.: Accelerating glacier mass loss on Franz Josef Land, Russian Arctic, Remote Sens Environ, 211, 357–375, https://doi.org/10.1016/j.rse.2018.04.004, 2018.

Zlotnicki, V., Wahr, J., Fukumori, I., and Song, Y. T.: Antarctic circumpolar current transport variability during 2003-05 from GRACE, J Phys Oceanogr, 37, 230–244, https://doi.org/10.1175/JPO3009.1, 2007.

Appendix A: Constraint sigmas for related CSR mascon series

The "sigmas" of the CSR mascon constraints have been changed substantially over the Arctic Ocean, during the various RL06 releases. For clarification, we show the changes between RL06.1, RL06.3 (identical to RL06.2), and the new RL06.2DO, in

https://doi.org/10.5194/essd-2025-718
Preprint. Discussion started: 15 January 2026

terms of climatologies. Note that, unlike the other two cases, the RL06.2DO mascons do not use the actual climatology shown, but instead have different values for each individual month (e.g., Fig.2 in the main text).

The CSR RL06.1 Arctic Ocean mascon constraints were in part defined by a 12-month climatology based on CSR RL05 mascons computed over the whole GRACE mission (Fig. A1). This input data, which defined the constraint sigmas, unfortunately contained residual north/south striations caused by GRACE/FO's orbital errors, which were later found to propagate into the RL06.1 mascon series.

The CSR RL06.2 and RL06.3 Arctic Ocean mascon constraints thus exclude this GRACE-based climatology, using only a 12-month climatology defined by the GAD values from the AOD1B product, which cannot contain GRACE-style stripe errors. A lower-bound for the constraint sigmas was set to 3 cm (to prevent the GAD series from understating real signal) and an upper-bound set to 5 cm. This removed the unrealistic Arctic striations, while still allowing the constraints to vary realistically and seasonally (Fig. A2).

The CSR RL06.2DO Arctic Ocean mascon constraints are defined as the minimum of two values: 1) the absolute value of the specific month's local GAD value, or 2) the climatological value for that calendar month. On top of this, we applied the same 3-5 cm bound on the constraint sigmas in all Arctic mascons, to eliminate cases where there would either be too little or too much constraint flexibility. The result is a set of constraints which varies uniquely for each month, rather than following a strict climatology (Figs. 2 and A3). Overall, this tends to tighten the constraints along the coasts of northern Eurasia. It does not notably alter the constraints compared to RL06.3 in areas away from the coastlines.

(We note that the technique used to estimate the RL06.2DO sigmas can potentially lead to undesirably reduced sigmas in cases when a month's GAD signal is atypically high compared to the climatology. The monthly value will then be ignored, in favor of the lower climatology value. In practice, however, the GAD climatology is typically at or above the 5 cm limit along the coastlines where sigmas are above the 3 cm minimum – see Fig A2 – such that this is rarely a problem.)

https://doi.org/10.5194/essd-2025-718
Preprint. Discussion started: 15 January 2026

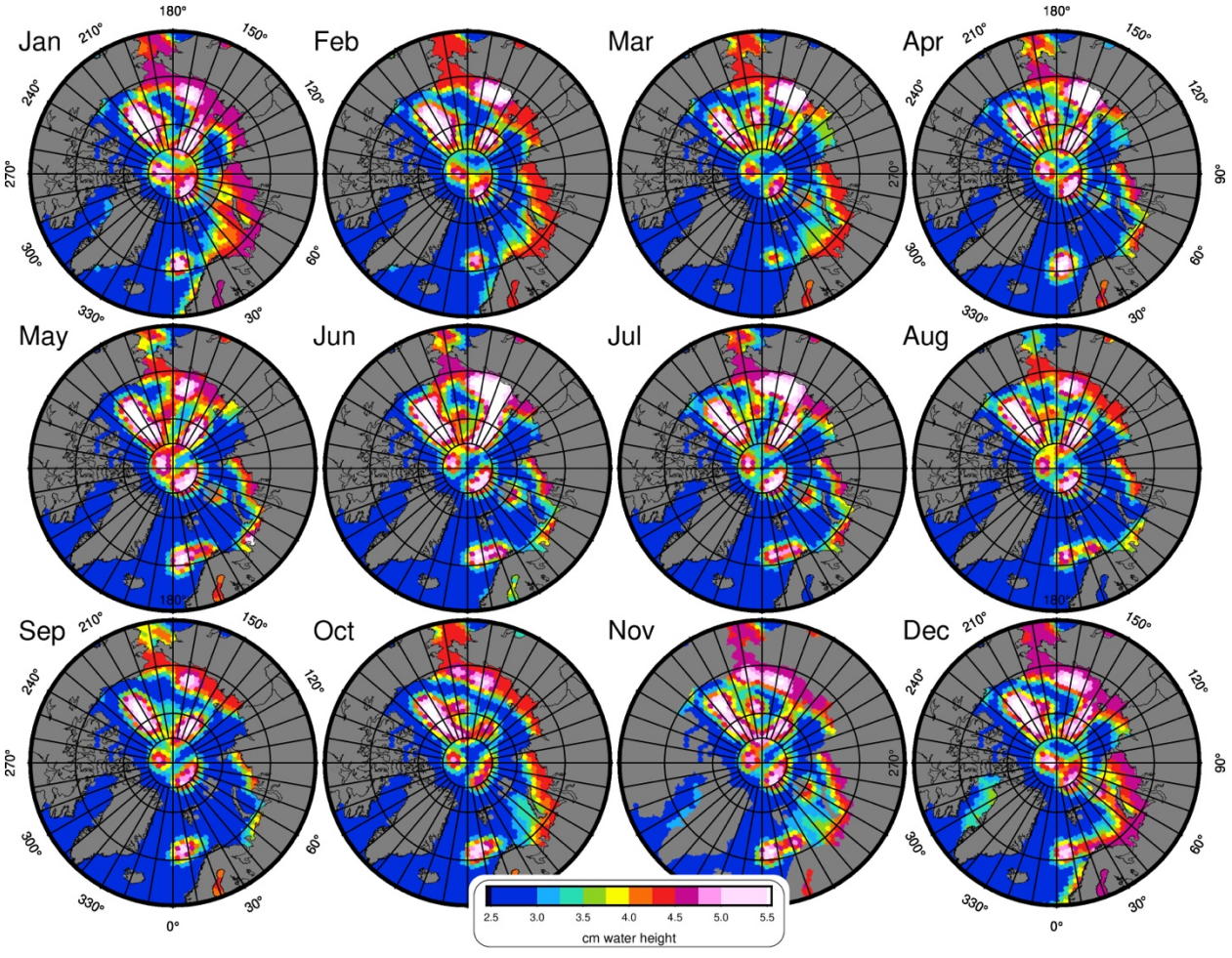

Figure A1: Arctic ocean climatology of CSR RL06.1 constraint sigmas. This is based on RL05 CSR mascons and contains "stripe-like" values in the arctic which do not realistically represent ocean variance.

https://doi.org/10.5194/essd-2025-718
Preprint. Discussion started: 15 January 2026

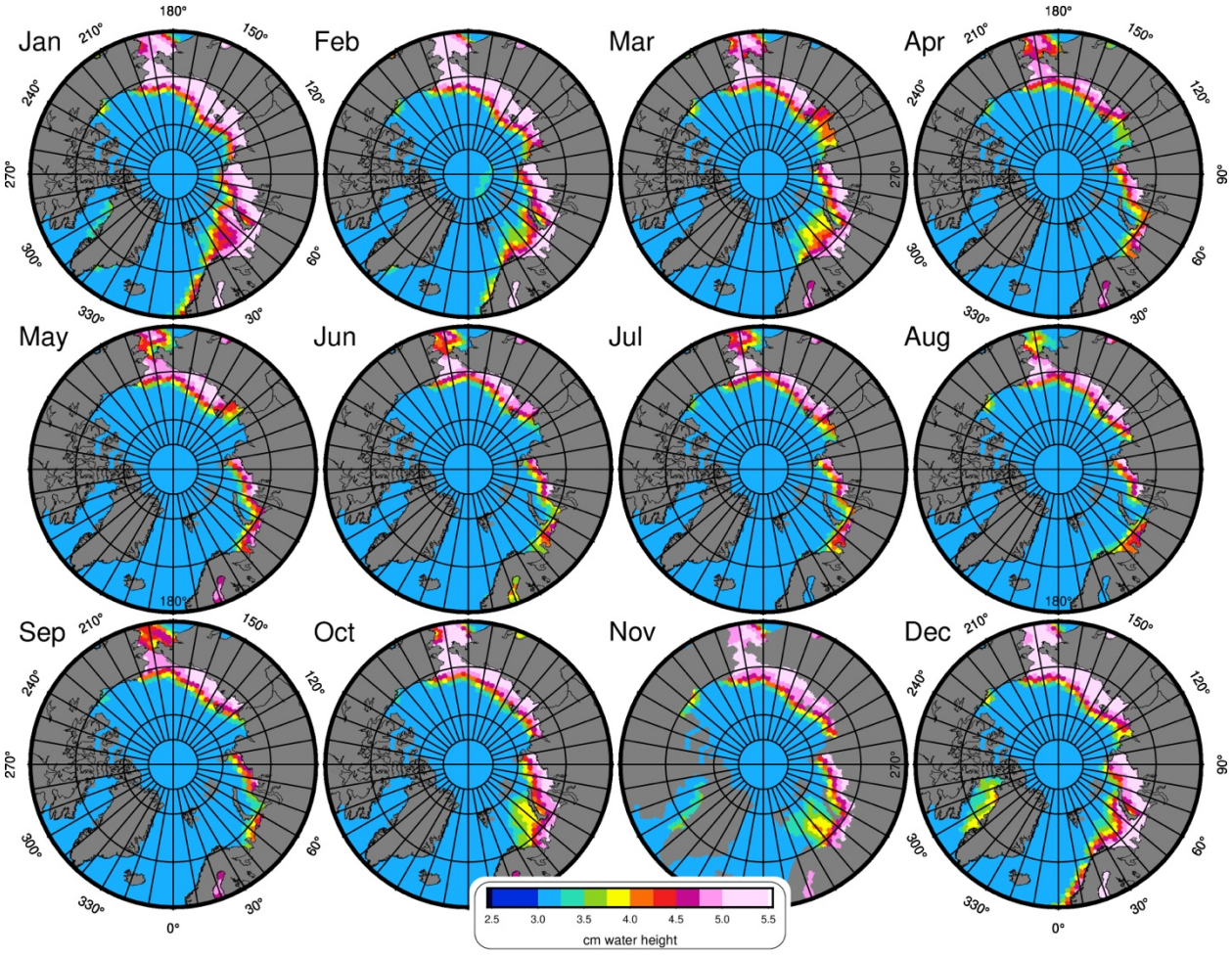

765 **Figure A2: Arctic ocean climatology of CSR RL06.3 constraint sigmas. This is based on the GAD climatology, with min/max boundaries of 3-5 cm.**

https://doi.org/10.5194/essd-2025-718
Preprint. Discussion started: 15 January 2026

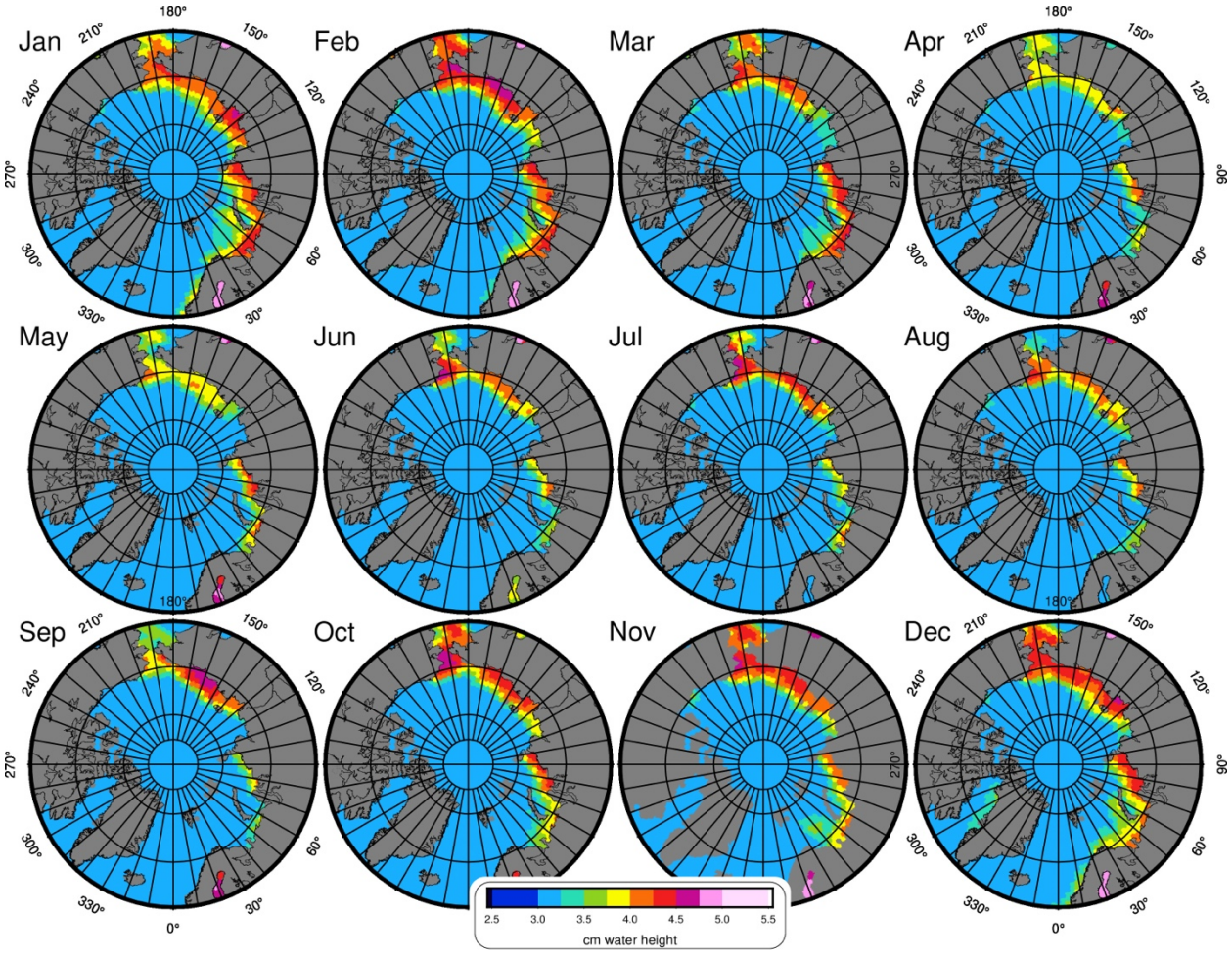

770 **Figure A3: Arctic ocean climatology of CSR RL06.2DO constraint sigmas. The DO sigmas are not a strict climatology, but vary uniquely each month. Shown is the average value per month over the 2002-2024 series, which can be more easily compared to Fig. A1 and A2.**